AN ABSTRACT OF THE THESIS OF

LYNN DALE TREMBLY for the Ph.D. in GEOPHYSICS
(Name) (Degree) (Major)

Date thesis is presented November 8, 1967

Title: SEISMIC SOURCE CHARACTERISTICS FROM EXPLOSION GENERATED P WAVES

Abstract approved Redacted for Privacy
Joseph W. Berg, Jr.

The earth-receiver system is considered as a lumped system. The operator which describes this system includes the effects of: (1) the source environment, (2) the propagation path to the station, and (3) the seismograph at the station. A method is presented whereby a seismograph station can be calibrated by an explosion at a given site using the seismic waves observed near the explosion (input signal) and at the station (output signal). Output signals recorded at that station can then be used to derive information about other sources for which this calibration applies. This method of calibration is applied to the primary waves from six underground nuclear explosions recorded by short-period vertical seismographs located at near-regional, regional, and teleseismic distances.

The principal constraints that limit the capabilities of the calibration method are: (1) The source-propagation path-receiver system acts as a filter which limits the amount of source-related information contained in the output signals; (2) The contamination of the primary waves by secondary arrivals limits the time duration of the output signals that can be used; and (3) The lumped operators for the earth-receiver systems may vary significantly for different explosions due to differences in the locations of the sources.

Information about the sources can be derived from distant signals for frequencies reliably related to the source, only. For the data used in this research, the low-frequency cutoff was 0.2 cps at all stations and the high-frequency cutoffs were 4.0, 3.0, and 2.0 cps at the near-regional, regional, and teleseismic distances. The low-frequency cutoff was due mainly to the recording instruments, and the high-frequency cutoffs were due to the attenuation of the seismic energy by the earth. The waveforms of the derived source functions were all similar due to the limited amount of high-frequency energy propagated to the distant stations. The most significant source information derived was the source energy in the above

frequency passbands. The most reliable results were obtained when three half-cycles of the observed output signals (first arrivals) were used. Differences between derived and "observed" source energies were mainly due to near-source propagation losses for the different explosions. When explosions in granite were used as calibration sources, the energies derived for explosions in tuff, alluvium, and dolomite media were 88, 65, and 12 percent of the respective "observed" source energies.

SEISMIC SOURCE CHARACTERISTICS FROM EXPLOSION GENERATED P WAVES

by

LYNN DALE TREMBLY

A THESIS

submitted to

OREGON STATE UNIVERSITY

in partial fulfillment of

the requirements for the

degree of

DOCTOR OF PHILOSOPHY

June 1968

APPROVED:

Redacted for Privacy

Professor of Geophysics
In Charge of Major

Redacted for Privacy

Chairman, Department of Oceanography

Redacted for Privacy

Dean of Graduate School

Date thesis is presented November 3, 1969

Typed by Elaine R. Justice for Lynn Dale Trembly

ACKNOWLEDGEMENTS

The work presented in this thesis was performed under the direction of Dr. Joseph W. Berg, Jr., Professor of Oceanography at Oregon State University until September 1966 and now Executive Secretary of the Earth Sciences Division of the National Academy of Sciences in Washington, D.C. I wish to express my gratitude to Dr. Berg for his assistance in selecting this project and for his many helpful suggestions in analyzing the data and in writing this thesis.

I would also like to thank Dr. Wayne V. Burt, Chairman of the Department of Oceanography at Oregon State University. Dr. Burt was my major Professor from September 1966 to November 1967.

Appreciation is extended to the Sandia Corporation, the Stanford Research Institute, the Department of Mines and Technical Surveys of the Dominion Observatory of Canada, and to the Seismic Data Laboratory in Alexandria, Virginia, for supplying the seismograms used in this thesis.

From September 1963 to September 1964, I was a recipient of a scholarship memorial to Mr. Raiford H. Burton

awarded through the Society of Exploration Geophysicists. From September 1964 to September 1966, I was a recipient of a National Aeronautics and Space Administration fellowship. I am grateful for this assistance.

This research was entirely supported by the Air Force Office of Scientific Research under Grant AF-AFOSR-62-376 as part of the Vela Uniform Program directed by the Advanced Research Projects Agency of the Department of Defense.

TABLE OF CONTENTS

LIST OF TABLES

LIST OF FIGURES

Figure | Page

SEISMIC SOURCE CHARACTERISTICS FROM EXPLOSION GENERATED P WAVES

INTRODUCTION

General discussion of the problem

The immediate objective of this research was to determine the amount of information about the seismic source signals generated by underground nuclear explosions that could be recovered from the initial seismic waves, P, recorded at near-regional to teleseismic distances.

Seismic body waves from earthquakes have been used to study the earth's interior since the early part of this century, and much has been learned about the nature of the earth. However, the study of the earth's interior has necessarily been complicated by the uncertainties about the signals introduced into the earth by the sources (Bullen, 1963). For natural events such as earthquakes for which the locations, depths, and origin times are not always precisely known, the utilization of amplitude information to determine source and propagation effects is complicated by uncertainties in the radiation patterns at the source and the path of energy transmission. With the

advent of underground nuclear explosions, emphasis was placed upon documenting the seismic waves at all epicentral distances (near-source to teleseismic) with precisely calibrated receivers. For these sources, the location, depth, and origin time can be precisely controlled so as to reduce some of the complications inherent with natural events. Thus, experimental conditions are nearly ideal for utilizing the recordings of nuclear explosions to determine how much information about the source is retained in the initial seismic wave (P) propagating to different epicentral distances.

The relationship between the initial seismic wave (primary wave) recorded at a seismograph station (output signal) and the seismic signal at the source (input signal) is illustrated in Figure 1 below. The earth-receiver system includes all of the effects of the source environment,

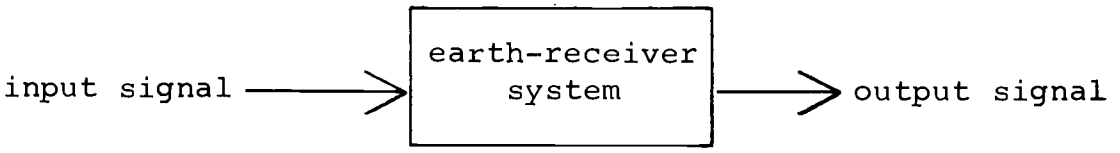

Figure 1. Block diagram showing the relation of the seismic waves recorded at distance to the seismic signal at the source.

propagation path, and the recording instruments. Gutenberg (1944) pointed out that, in principle, the seismic waves at distance may be predicted if the velocity structure and the attenuation within the earth are known. This approach is essentially the problem of solving the wave equation with boundary conditions established by the physical properties of the earth. A solution in terms of particle displacement for a single frequency may be represented as shown in equation (1).

$$U(r,w) = \epsilon F(r) e^{-\alpha r} U_o(w), \qquad (1)$$

where: $U(r,w)$ = particle displacement at the distance r;

$U_o(w)$ = particle displacement at the source;

w = frequency in radians per second;

ϵ = factor representing the boundary losses (including free surface effects and instrument magnification);

$F(r)$ = geometrical spreading factor; and

α = factor representing the attenuation of the earth.

In general, each of the terms in equation (1) may be complex functions of frequency and are usually not completely known. Primarily, this is due to the inability to

completely define the boundary conditions applicable for a given propagation path. However, an alternate approach may be used to predict the primary waves at distance. The source conditions, propagation path, and recording instrument may be considered from the standpoint of a lumped system and the separate effects of each of the components of the system may be lumped into one operator as shown in equation (2).

$$U(r,w) = \left[H(w,r)\right] \left[U_o(w)\right], \qquad (2)$$

where H(w,r) is the lumped operator for the source-propagation path-receiver system. The problem then consists of determining the lumped calibration operator, H(w,r), by utilizing near-source and distant station recordings of seismic waves for a given explosion. If the recording station has been calibrated in this manner, it should be possible to derive source information from other distantly recorded signals. The purpose of this research was to determine the constraints involved in using lumped calibration operators to derive the seismic source information from signals recorded at different epicentral distances and to evaluate the capabilities of this method of calibration.

Basic Theory

A physical system, such as the earth-receiver system, operates on an excitation from an earthquake or an explosion so that the seismic signals recorded at distant seismograph stations represent the response of the system to the exictation (see Figure 1). In general, the response to every conceivable input signal must be known to describe completely any system, but a system can be calibrated for a limited set of signals. For the system under consideration, the assumptions of linearity, passitivity, stability, time invariance, and causality greatly simplify the specification of the system.

A system is linear if its operator is independent of the amplitude and waveform of the input signal. Although the extent to which the earth satisfies the linearity condition is not completely known, the assumption of linearity for the earth-receiver system is common and will be made in this research. A system is passive if the output signal is derived only from the source (i.e., if the system itself does not generate energy). The earth-receiver system is passive, but noise, such as microseisms, may cause it to appear nonpassive. If the signal due to

noise is large with respect to the source-related signal, the analysis of the response of the system is greatly complicated. A system is stable if the output signal as well as the input signal is bounded. A system is time invariant if its operator does not change with time. A causal system has the property that if the input signal is zero for time $t \leqslant t_1$ then the output signal must be zero for time $t \leqslant t_1 + T$, where T is the time required for the signal to propagate through the system. These three conditions are satisfied by the earth-receiver system.

Papoulis (1962) discussed the above properties and expressed the response, $f_{out}(t)$, of such a system to an excitation, $f_{in}(t)$, as the convolution integral

$$f_{out}(t) = h(t) * f_{in}(t) = \int_o^t h\,(t - \lambda)\; f_{in}(\lambda)\; d\lambda, \quad (3)$$

where: $f_{out}(t)$ = output function of time;

$h(t)$ = impulse, $\delta(t)$, response of the system;

and

$f_{in}(t)$ = input function of time.

If $f_{in}(t)$, $h(t)$, and $f_{out}(t)$ are Fourier transformable then each term in equation (3) may be written in the frequency (w) domain for a given distance, r, in terms of the Fourier transform as shown in equations (4), (5), and (6).

$$F_{in}(w) = \left|F_{in}(w)\right| \; e^{i\theta_{in}(w)} = \int_{-\infty}^{\infty} f_{in}(t)\, e^{-iwt}\, dt \qquad (4)$$

$$F_{out}(w) = \left|F_{out}(w)\right| \; e^{i\theta_{out}(w)} = \int_{-\infty}^{\infty} f_{out}(t)\, e^{-iwt}\, dt \qquad (5)$$

$$H(w) = \left|H(w)\right| \; e^{i\phi_{H}(w)} = \int_{-\infty}^{\infty} h(t)\, e^{-iwt}\, dt, \qquad (6)$$

where:

w = frequency in radians per second;

$i = (-1)^{\frac{1}{2}}$;

$\left|F_{in}(w)\right|$ = modulus of the Fourier transform of the input signal, $f_{in}(t)$;

$\theta_{in}(w)$ = phase relation of the Fourier transform of $f_{in}(t)$;

$\left|F_{out}(w)\right|$ = modulus of the Fourier transform of the output signal, $f_{out}(t)$;

$\theta_{out}(w)$ = phase relation of the Fourier transform of $f_{out}(t)$;

$\left|H(w)\right|$ = modulus of the Fourier transform of the impulse response of the system, $h(t)$; and

$\phi_{H}(w)$ = phase relation of the Fourier transform of $h(t)$.

Equation (3) is written in the frequency domain as shown in equations (7) and (8).

$$\left|F_{out}(w)\right| = \left|H(w)\right| \left|F_{in}(w)\right| \tag{7}$$

$$\theta_{out}(w) = \phi_H(w) + \theta_{in}(w). \tag{8}$$

Equations (7) and (8) are equivalent to the operator equation written in equation (2) where $\left|H(w)\right|$ and $\phi_H(w)$ correspond to the amplitude and phase of the lumped calibration operator for the earth-receiver system. Therefore, if the calibration operator were known, then the spectrum of a distantly recorded signal could be used to determine the amplitude and phase of the source spectrum as shown in equations (9) and (10).

$$\left|F_{in}(w)\right| = \left|\frac{F_{out}(w)}{H(w)}\right| \tag{9}$$

$$\theta_{in}(w) = \theta_{out}(w) - \phi_H(w). \tag{10}$$

The problem of using equations (9) and (10) to describe the spectra of source signals from recorded output signals then becomes one of correctly describing the calibration operator, $\left|H(w)\right| e^{i\phi_H(w)}$, and defining the constraints which limit the use of the operator.

Approach to the problem

One approach to formulating a mathematical calibration operator has been to separate the operator into components which correspond to each portion of the path transversed by the seismic waves in going from the source through the receiver as shown in Figure 2.

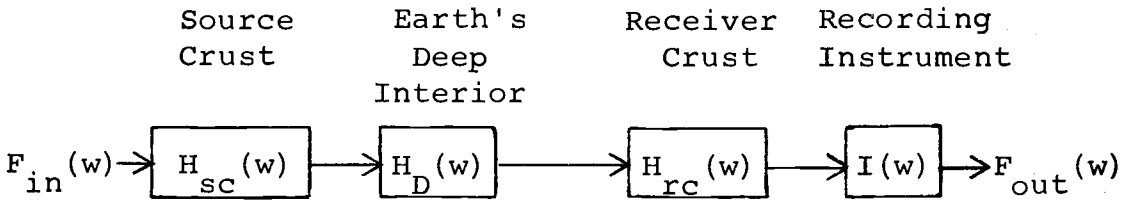

Figure 2. Block diagram showing the components of the lumped calibration operator for the earth-receiver system.

Each of the individual components has an operator associated with it which is, in general, a complex function of frequency. If expressions could be written for each of the individual components of the system, then the signal recorded at the station could be traced backwards from the recording station to the source by correcting for each component which took part in shaping the waveform of the signal. If this approach is taken, then equations (9) and (10) are expressed as shown in equations (11) and (12).

$$\left|F_{in}(w)\right| = \frac{\left|F_{out}(w)\right|}{\left[\left|H_{sc}(w)\right| \left|H_{D}(w)\right| \left|H_{rc}(w)\right| \left|I(w)\right|\right]} \qquad (11)$$

$$\Theta_{in}(w) = \Theta_{out}(w) - \left[\phi_{sc}(w) + \phi_{D}(w) + \phi_{rc}(w) + \phi_{I}(w)\right]. \qquad (12)$$

Therefore, the calibration operator for a given propagation distance, r, would be the product (in the frequency domain) of the individual components as shown in Figure 2 and as given in equations (11) and (12). However, such an approach does not consider the earth-receiver system as a lumped system, and mathematical expressions for each of the separate components of the operator must be formulated.

Fuchs (1966) gave the source crust operator, $H_{sc}(w)$, for body waves from three types of point sources located in a flat-lying layered crust overlying a homogeneous half-space. Haskell (1962) gave a matrix formulation for the effects of the earth's crust at the recording station, $H_{cr}(w)$. The receiver operator, $I(w)$, is normally well known (Bogert, 1962). Ben-Menahem, Smith, and Teng (1965) used Haskell's crustal operator and operators for the earth's deep interior, $H_{D}(w)$, which included the effects of geometrical spreading and attenuation, to correct

long-period P wave signals to determine the source parameters of earthquakes. Toksöz, Ben-Menahem, and Harkrider (1964) applied a similar technique for seismic surface waves to determine the parameters of explosions. However, Teng and Ben-Menahem (1965) indicated that for periods less than ten seconds the operators were not applicable, and that long-period body waves did not serve as an efficient tool with which to estimate source characteristics for explosions or earthquakes of magnitude less than seven. In order to apply this technique to seismic waves of frequency greater than 0.1 cps, the geology, at the source and recording station, and the propagation path effects would have to be known more accurately than is now commonly the case. For example, the attenuation and geometrical spreading terms are difficult to formulate accurately for high frequencies due to incomplete knowledge of the velocity structure and the absorptive character of the earth's interior. Also, the geological structures at recording stations are not normally known to the extent needed to formulate a crustal operator. Therefore, this approach to solving the problem of describing source parameters from distant seismic signals is severely limited when applied to seismic waves of

frequencies greater than 0.1 cps.

The approach used in this research was to "calibrate" a recording station using the source signal observed near an explosion and an output signal recorded at the station. That is, if the signal both at the source and at the receiver are known for one source then the calibration operator can, in principle, be determined as shown in equations (13) and (14). In order to avoid confusion in the following discussion, the Fourier transforms of the input and output signals of the calibration source are denoted by $C_{in}(w)$ and $C_{out}(w)$, respectively, and the Fourier transforms of the input and output signals for the unknown sources are denoted by $U_{in}(w)$ and $U_{out}(w)$, respectively.

$$\left|H(w)\right| = \left|\frac{C_{out(w)}}{C_{in}(w)}\right| \tag{13}$$

$$\phi_H(w) = \theta_{out}(w) - \theta_{in}(w) \tag{14}$$

where: $\left|C_{in}(w)\right|$ = the amplitude spectrum of the input signal from the calibration source;

$\theta_{in}(w)$ = the phase spectrum of the input signal from the calibration source;

$\left|C_{out}(w)\right|$ = the amplitude spectrum of the output signal from the calibration source; and

$\Theta_{out}(w)$ = the phase spectrum of the output signal from the calibration source.

Then for any other distant signal for which the calibration applies, a source spectrum can be derived using the distant signals as shown in equations (15) and (16).

$$\left|U_{in}(w)\right| = \frac{\left|C_{in}(w)\right| \left|U_{out}(w)\right|}{\left|C_{out}(w)\right|} \tag{15}$$

$$\Psi_{in}(w) = \Theta_{in}(w) - \Theta_{out}(w) + \Psi_{out}(w) \tag{16}$$

where: $\left|U_{in}(w)\right|$ = the amplitude spectrum of the input signal from the unknown source;

$\Psi_{in}(w)$ = the phase spectrum of the input signal from the unknown source;

$\left|U_{out}(w)\right|$ = the amplitude spectrum of the output signal from the unknown source; and

$\Psi_{out}(w)$ = the phase spectrum of the output signal from the unknown source.

The seismic energy and the waveform of the unknown source signal can then be computed. For example, the waveform of the unknown source signal can be obtained from the derived spectrum by using the inverse Fourier transform of $\left|U_{in}(w)\right| \; e^{i\Psi_{in}(w)}$, as shown in equation (17).

$$u_{in}(t) = T^{-1}\left\{\frac{|C_{in}(w)|\ |U_{out}(w)|}{|C_{out}(w)|}\exp\left[i(\theta_{in}(w) - \theta_{out}(w) + \psi_{out}(w))\right]\right\}, \qquad (17)$$

where $T^{-1}\{\ \}$ denotes the inverse Fourier transform of the quantity in brackets. Equations (15), (16), and (17) define the method of calibration to be evaluated in this research.

The most obvious requirement of this approach is that to calibrate a recording station both the seismic signal at the source (input signal) and the signal at the station (output signal) must be known for an event. Measurements of ground motion in the proximity of the elastic-inelastic boundaries of several underground explosions are available which offer the best opportunity to date to describe the input signal to the earth system for any seismic event.[1] In this research, the seismic waves from six underground explosions were analyzed with respect to the use of the calibration method to describe seismic source characteristics.

---

1. The elastic-inelastic boundary effects to the radius of the equivalent cavity which separates the inelastic region surrounding an explosion from the elastic region in which strains can be approximated using infinitesimal strain theory, either purely elastic or allowing for frictional losses (Kisslinger, 1963).

It is well known that information is filtered from signals propagated through the earth-receiver system and therefore limitations on the completeness of the source-related information contained in the output signals represent a constraint on the method of calibration. Closely associated with the constraint of the incompleteness of the output information is the constraint due to the effects of noise which may contaminate the output signals, where noise is defined as any information which is not source-related.

For point sources in an infinite homogeneous medium, the compressional waves generated by explosions and the signals recorded within the medium would be directly related as was shown in Figure 1. However, the earth is a finite and heterogeneous medium, so the compressional wave generated by an explosion is the source of several types of waves recorded at the distant stations. The seismograms recorded at the seismograph stations, therefore, consist of many arrivals which have propagated to the stations by different paths. Some of these waves interfere with the initial P waves and this makes it difficult to define the first arrival on the records, which is another constraint on the calibration method. In this

research different durations of the first arrivals (primary waves) were used as the output signals, and the effects of the duration of the output signals on the method were considered.

Since the geology of the near-source region contributes to the lumped calibration operator, changes in the operator due to differences in source conditions represent another constraint on the method of calibration. Underground nuclear explosions may differ in location, depth, medium, and/or size. The extent to which these factors affect the use of the lumped calibration operator is considered in the analysis.

The investigation of the constraints that were involved in the application of the calibration method was confined to first arrivals generated by underground nuclear explosions. The initial motion was clearly identifiable at the recording stations. Since uncertainties about the input and output signals were minimized for the data used, the constraints investigated were those associated with the best quality seismic data that were available.

DATA

Seismic data from six underground nuclear explosions were used in this research. Pertinent information about the explosions is given in Table I. The locations of the explosions are shown in Figure 3. All of the explosions except Shoal were located within the Nevada Test Site (NTS), and the geology of the NTS was described by Johnson and Hibbard (1957), McKay (1962), and Springer (1966). The location of the Shoal explosion was approximately 300 kilometers north of the NTS in the Sand Springs Range of central Nevada, and the geology of the area was described by the Nevada Bureau of Mines (1962).

Particle velocity as a function of time was measured at shot depth in the elastic region near the elastic-inelastic boundaries of the Hardhat, Haymaker, Shoal and Handcar explosions.[2] The subsurface instruments were

2. The subsurface records from all of the explosions except Hardhat were obtained from the Sandia Corporation through the courtesy of William Perret and Wendell Weart. The subsurface recording from the Hardhat explosion was obtained from the Stanford Research Institute through the courtesy of Larry Swift.

TABLE I. Information about the explosions.

Explosion Name	Date	Time of Detonation (GCT)	Explosion North Latitude	Coordinates West Longitude	Type of Medium	Shot Depth (km)	Yield (Ktons)*
Hardhat	2/15/62	18:00:00.10	37 13'35"	116 03'34"	granite	0.29	5.9
Haymaker	6/27/62	18:00:00.12	37 02'30"	116 02'07"	alluvium	0.41	56
Bilby	9/13/63	17:00:00.13	37 03'38"	116 01'18"	tuff	0.70	220
Shoal	10/26/63	17:00:00.12	39 12'01"	118 22'49"	granite	0.37	12
Handcar	11/5/64	15:00:00.10	37 10'28"	116 04'01"	dolomite	0.40	10
Pile Driver	6/2/66	15:30:00.10	37 13'37"	116 03'20"	granite	0.46	

*One kiloton (Kton) is defined as a total energy release of 10^{12} calories $= 4.2 \times 10^{19}$ ergs, (Johnson et al 1959).

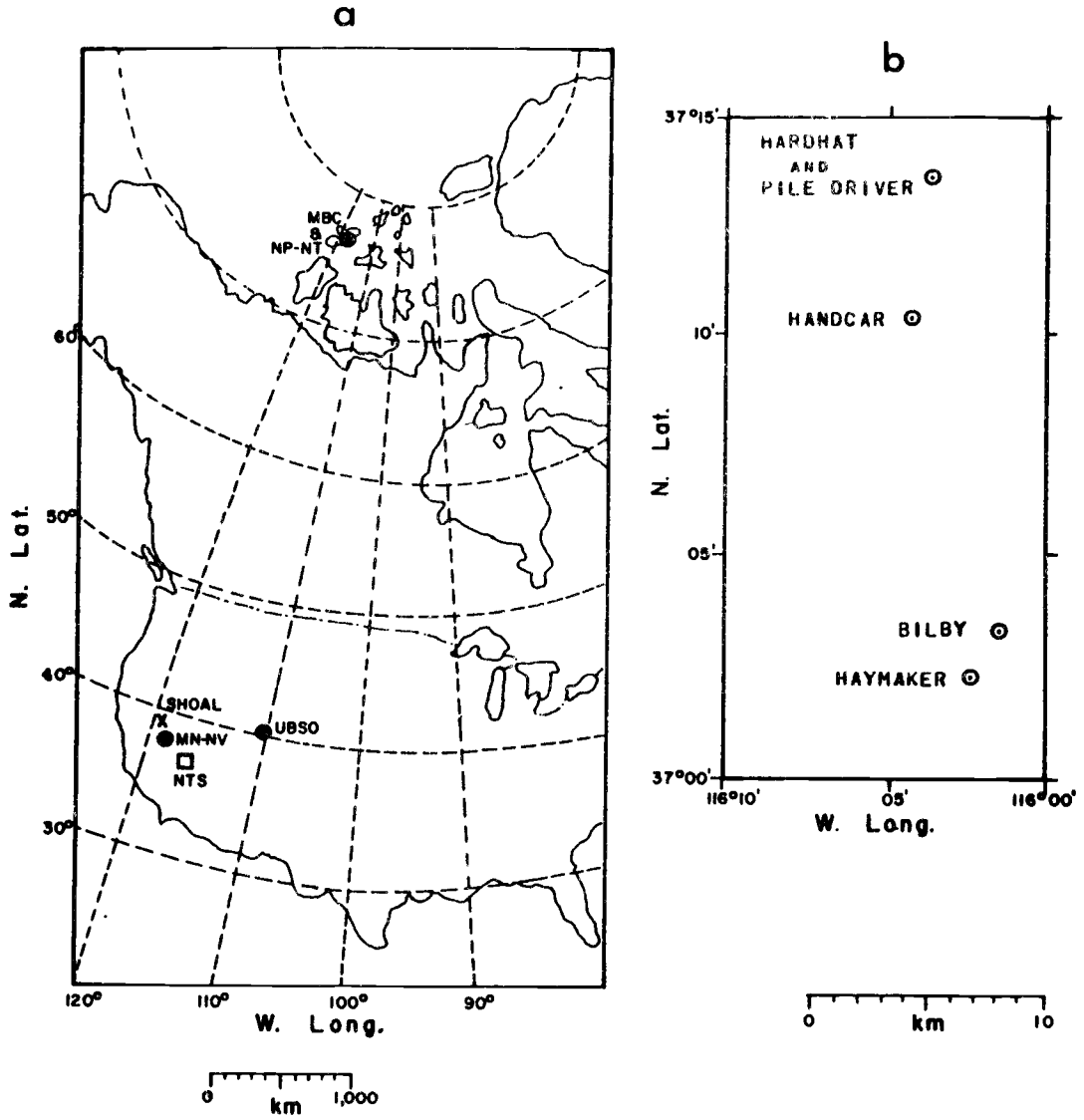

Figure 3. (a) Map showing the locations of the Shoal nuclear explosion, Nevada Test Site (NTS), and recording stations.
(b) Enlargement showing the locations of the explosions within the Nevada Test Site.

described by the Sandia Corporation (1963, 1965). The frequency response of the instruments was constant in the frequency range $0.1 \leqslant f \leqslant 300$ cycles per second (cps), and the dynamic range of the instruments was from 3.0×10^0 to 1.8×10^4 cm/sec (Sandia Corporation, 1965). The locations of the subsurface instruments used for the Haymaker and Shoal explosions were described by Trembly and Berg (1966) and Swift (1962) described those for the Hardhat explosion. No data have been published about the locations of the subsurface instruments near the Handcar explosion. The radial component of the particle velocity measured by the subsurface instruments at shot depth in the proximity of the elastic-inelastic boundaries of the Hardhat, Handcar, Shoal, and Haymaker explosions are shown in Figure 4.[3] The range, r, of each of the subsurface instruments from the explosions and the compressional wave propagational velocity, c, observed in the vicinity of each explosion are shown in the figure.

---

3. There were subsurface instruments at shot depth and at a range of 0.59 kilometers in three quadrants around the Shoal explosion and azimuthal assymmetry in the seismic wave pattern was observed (Trembly and Berg, 1966). Only the recording in the northeastern quadrant was used in this research because all of the distant recording stations used were in that quadrant from the explosion .

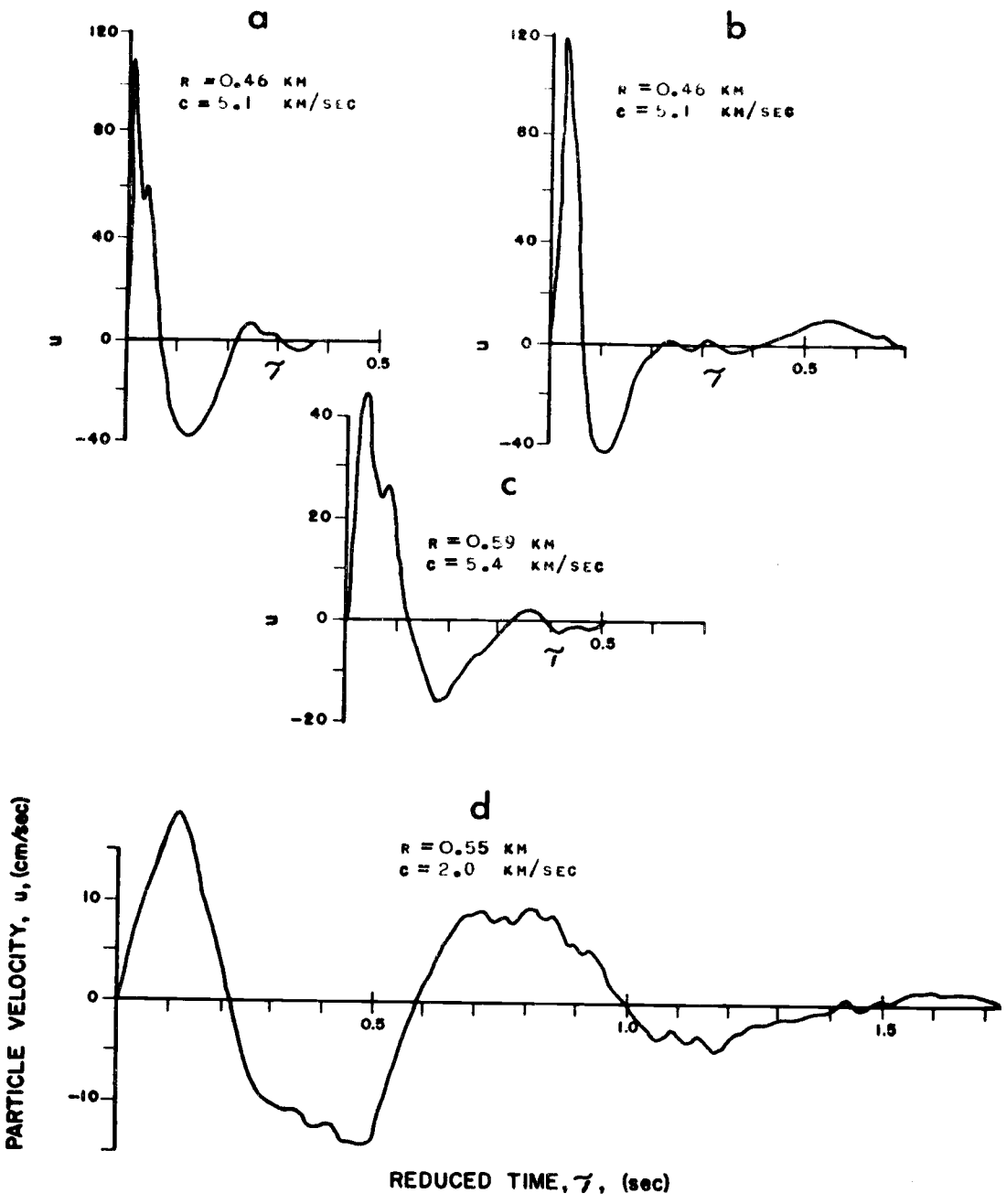

Figure 4. Particle velocity waveforms at the subsurface stations near the explosions: Hardhat, (b) Handcar, (c) Shoal, and (d) Haymaker. u = particle velocity in (cm/sec)
τ = reduced time in seconds

Information pertaining to the distant seismograph stations, from which records of the seismic events were used for this research, is summarized in Table II, and the locations of the stations are shown in Figure 3. The recording stations at Mina,(MN-NV) Nevada, and Mould Bay, (NP-NT) Canada are Long Range Seismic Measurements (LRSM) stations established under the VELA UNIFORM Program. The Uinta Basin Seismological Observatory (UBSO), Utah, is an observatory established under the VELA UNIFORM Program, also. The station at Mould Bay, Canada, denoted by MBC is a permanent seismograph station operated by the Department of Mines and Technical Surveys of the Dominion Observatory.

The amplitude response (particle velocity) and phase shift for the short-period vertical instruments at the stations MN-NV, UBSO, and NP-NT are shown in Figure 5 and are denoted LRSM.[4] These responses pertain to the complete systems and are determined from electromagnetic

4. The response curves for the instruments at stations UBSO and NP-NT may differ slightly from that shown in Figure 5 because different seismometers were used at these stations, but the difference would not affect the results of this research.

TABLE II. Information about the recording stations.

Station Name	Station Coordinates North Latitude	West Longitude	Explosion	Epicentral Distance (km.)	Traveltime (Sec.)
Mina, Nevada (MN-NV)	38 26'10"	118 08'53"	Hardhat	228	35.4
			Haymaker	242	37.6
			Bilby	242	37.1
			Handcar	231	35.7
			Pile Driver	228	35.4
Uinta Basin Observatory (UBSO)	40 19'18"	109 34'07"	Bilby	668	93.9
			Shoal	765	106.4
			Handcar	664	93.4
			Pile Driver	660	92.2
Mould Bay, Canada (NP-NT)	76 15'08"	119 22'18"	Bilby	4372	451.4
			Shoal	4131	434.3
			Pile Driver	4353	450.0
Mould Bay, Canada (MBC)	76 14'00"	119 20'00"	Haymaker	4372	451.5
			Bilby	4372	451.5
			Shoal	4131	434.3
			Handcar	4359	450.6
			Pile Driver	4353	450.0

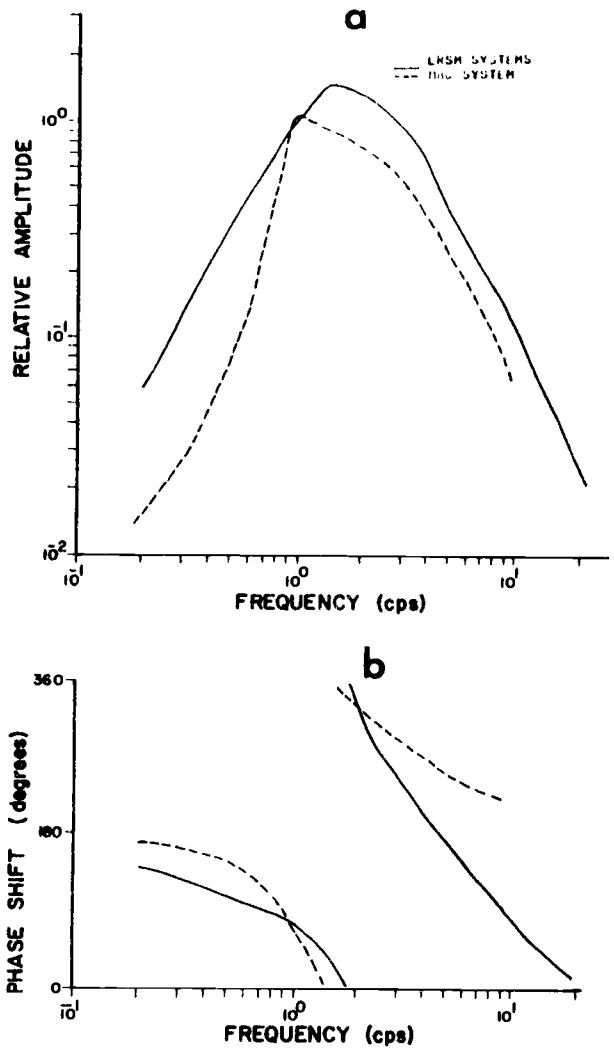

Figure 5. (a) Amplitude and (b) Phase-response curves of the short-period vertical recording systems at the LRSM stations (MN-NV, UBSO, and NP-NT), and the MBC station.

pulse, shake-table, and weight-lift tests. The amplitude responses for the LRSM systems may deviate from that shown in Figure 5 by ± 10 percent at 0.1 cps, zero percent at 1.0 cps, ± 7 percent at 3.0 cps, and ± 30 percent at 10.0 cps due to changes in the systems over extended periods of time. The recording systems are not considered to be reliable for frequencies above ten cps and are not routinely calibrated for those frequencies (Geotechnical Corporation, 1963). Data from these stations are recorded on magnetic tape as well as on 35 mm film.

The amplitude response (particle velocity) and phase shift of the short-period vertical recording system at station MBC are shown in Figure 5, also. The system response curves were not available for frequencies greater than ten cps. Seismic events were recorded on photographic paper at this station.

All of the output signals (distant recordings) used in this research are shown in Figure 6. The P wave signal was greater than the microseismic noise by approximately 10/1, for these recordings. The amplitudes on the records were normalized by dividing record amplitude for each event by the system magnifications at one cps. The accuracy of the magnification at one cps has been estimated

to be within ± 5 percent (Geotechnical Corporation, 1963).

The portions of the recordings shown in Figure 6 were digitized for the purpose of analyzing the data. All of the recordings except those from MBC were digitized from magnetic tape at 0.02 seconds time interval, whereas the paper recordings from MBC were digitized at the same time interval using a traveling microscope.[5] Both methods of digitization were accurate to approximately ± one percent of the peak normalized record amplitudes.

5. The recordings from the explosions Hardhat and Handcar at MN-NV, Bilby at UBSO, and Shoal and Bilby at NP-NT were digitized at 0.05 seconds time interval and interpolated to 0.02 seconds time interval. The Bilby recording at MBC was digitized for only 2.0 seconds of record before the seismogram was returned.

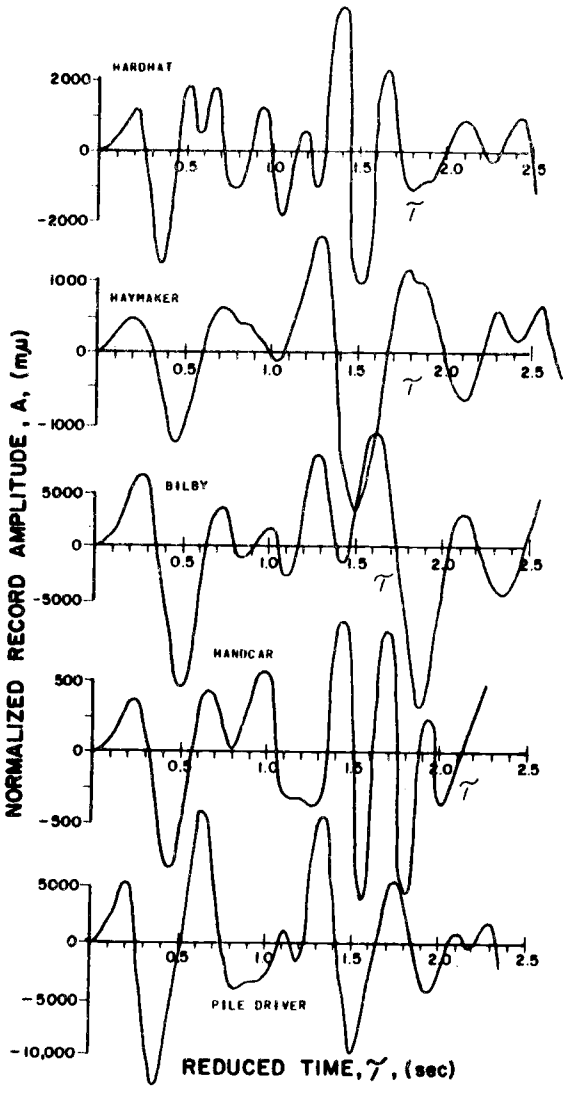

Figure 6a. The first arrivals recorded on the short-period vertical instrument at station MN-NV. A = normalized record amplitude in millimicrons (mμ). τ = reduced time in seconds.

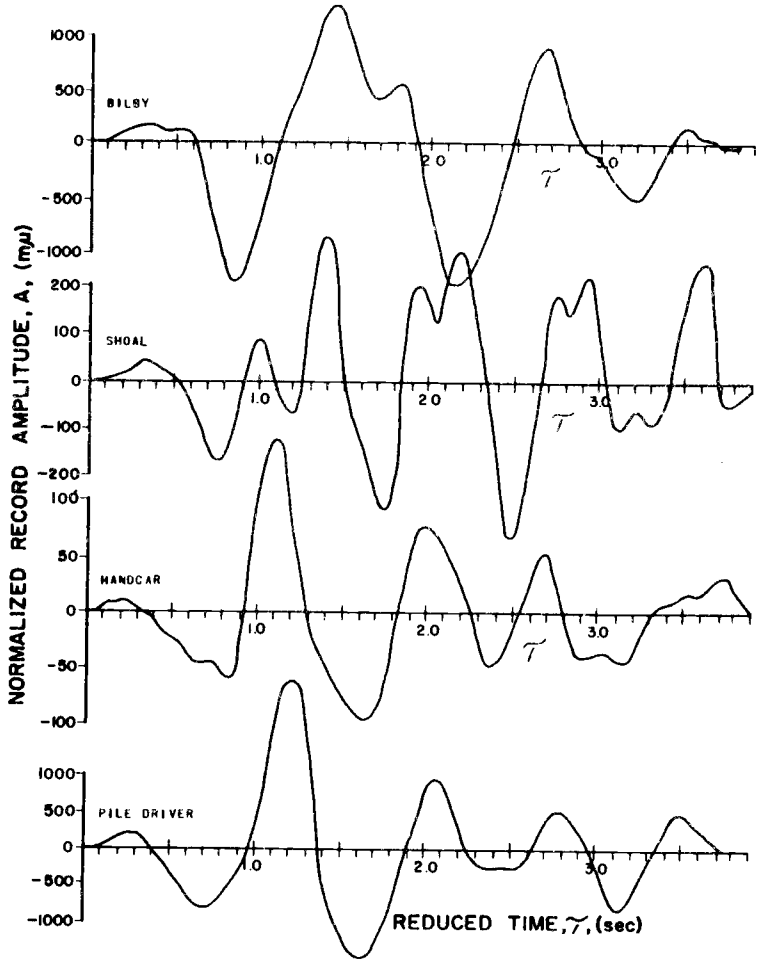

Figure 6b. The first arrivals recorded on the short-period vertical instrument at station UBSO. A = normalized record amplitude in millimicrons (mμ). τ = reduced time in seconds.

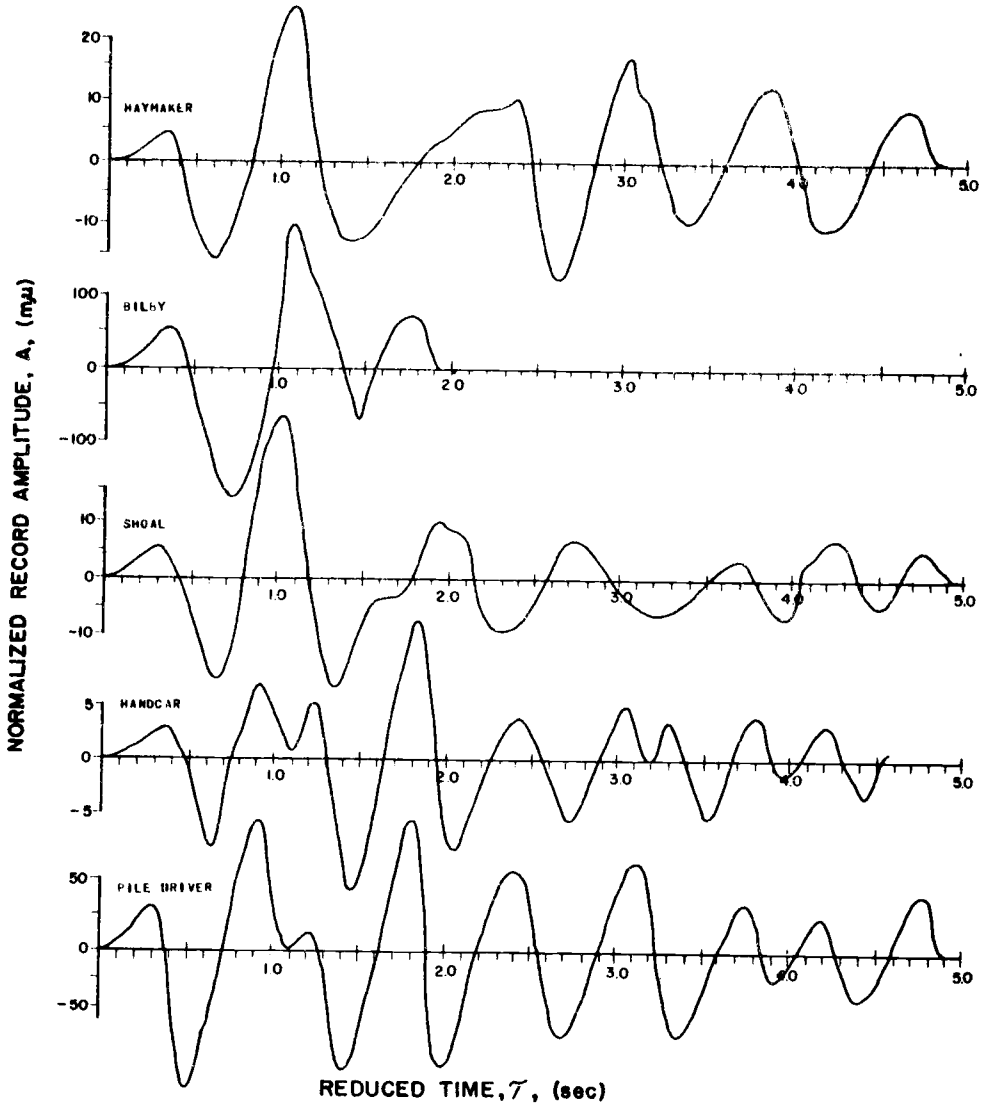

Figure 6c. The first arrivals recorded on the short-period vertical instrument at station MBC. A = normalized record amplitude in millimicrons (mμ). τ = reduced time in seconds.

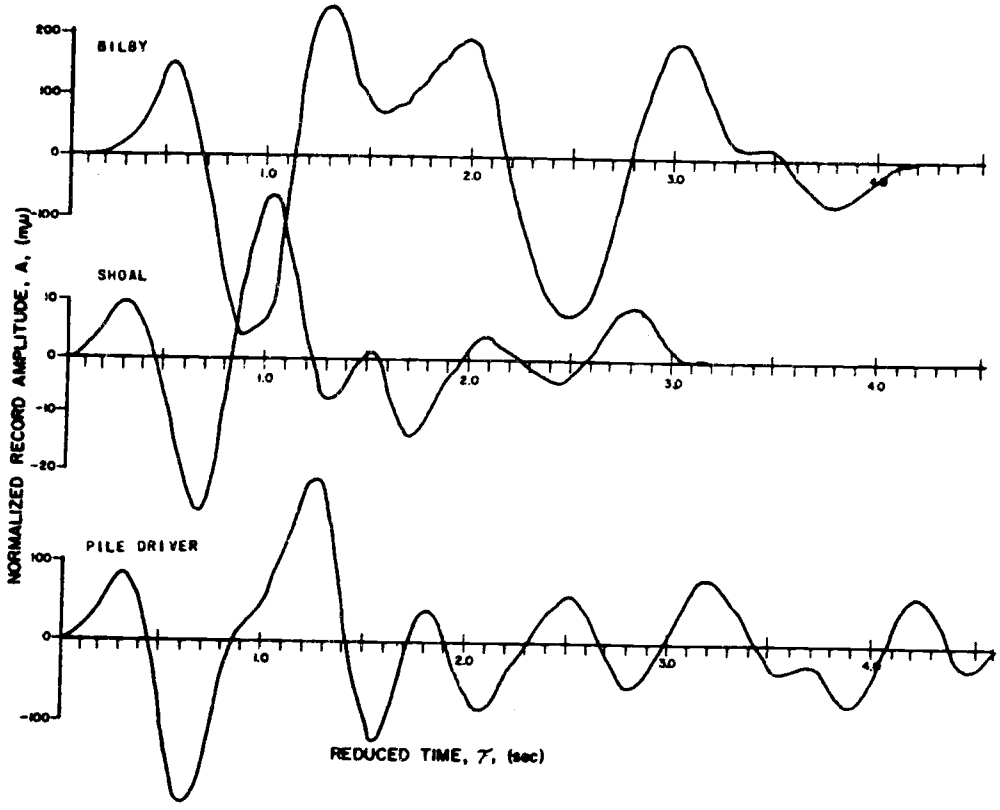

Figure 6d. The first arrivals recorded on the short-period vertical instrument at station NP-NT. A = normalized record amplitude in millimicrons (mμ). τ = reduced time in seconds.

ANALYSIS OF THE DATA

In this chapter, the distant stations are calibrated using known input and output signals, and source functions are derived using other seismic signals recorded at the stations. In the first section the near-source recordings are analyzed to obtain the observed source functions. The effects of the source medium, the free surface, and possible residual displacements near the sources are discussed. In the next section, the observed source functions are used to synthesize the initial waves at the distant recording stations to aid in determining more adequately the duration of the observed primary waves. In the final section an observed output signal is used in conjunction with an observed source function to derive the lumped calibration operator. The calibrated system (source-propagation path-receiver) is used to derive source functions from other output signals. The observed and derived source functions are compared as to waveform, frequency content, and energy. The constraints on the method of calibration are discussed.

Observed source functions

The particle velocity waveforms, radial component, shown in Figure 4 were recorded in the horizontal planes of the explosions. Since the source signal that propagates to large epicentral distances leaves the source at angles to the vertical other than 90 degrees, it is desirable to determine how indicative the waveforms in Figure 4 are of the source signals in the lower hemisphere of the explosion. The locations of the two subsurface recording stations near the Hardhat explosion that were used to make this comparison are shown in Figure 7a. The two recording stations were located in the same azimuth and at the same radial range, and the radial component of particle velocity was measured using the same type instruments in both cases. As shown in Figure 7a, station 2 was located at a 50 degree angle downward from a hypothetical horizontal plane through the explosion. The particle velocity waveforms recorded at the two stations are shown in Figure 7b. The pulses were quite similar in appearance, and the peak particle velocity amplitudes were equal within ten percent, which was within the accuracy of the subsurface data (Werth and Herbst, 1963).

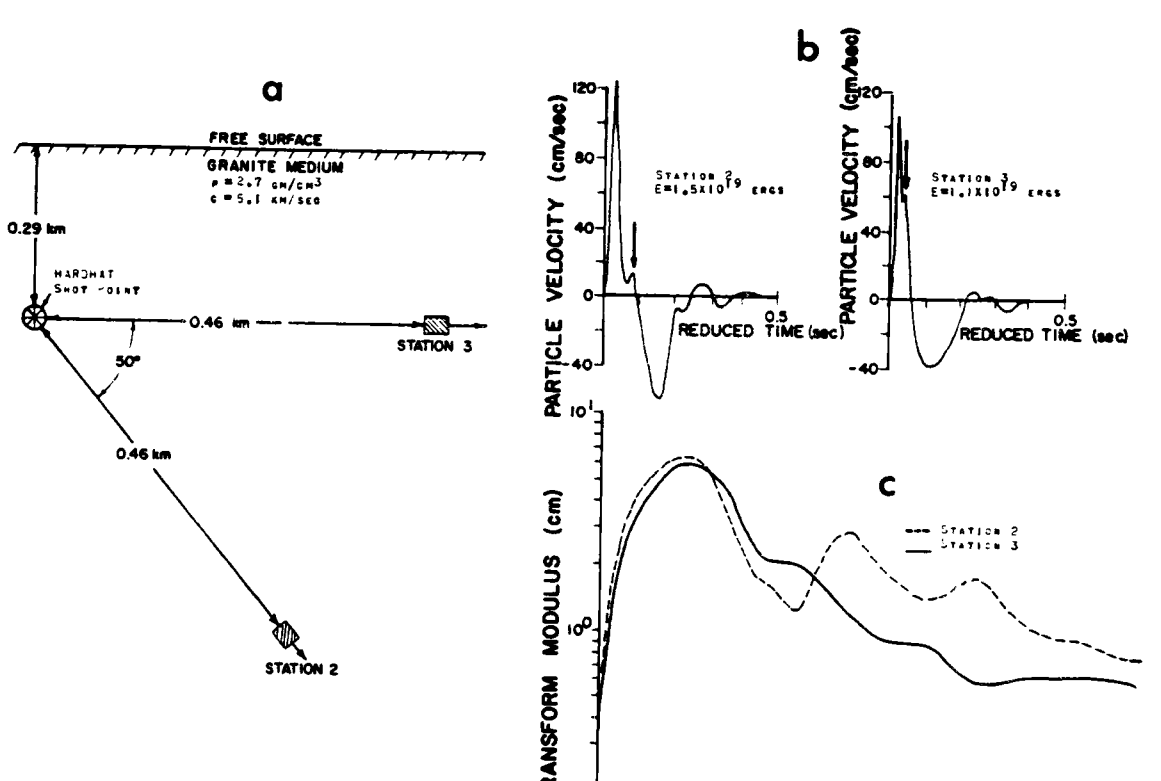

Figure 7. (a) Locations of the subsurface recording stations 2 and 3 near the Hardhat explosions, (b) Comparison of the near-source signals recorded at the two stations, and (c) Comparison of the spectral amplitudes.

The seismic energy of each of the waveforms was calculated using equation (18), (Howell and Budenstein, 1955).

$$E = 4\pi R^2 \rho c \Delta\tau \sum_j \left[v(\tau_j) \right]^2, \qquad (18)$$

where: R = the range of the station;

ρ = the density of the medium;

c = P wave propagational velocity;

τ = reduced time = time - travel time;

$\Delta\tau$ = digitizing interval; and

$v(\tau_j)$ = digitized seismic trace.

The energy represents the total seismic energy (kinetic plus potential) on a sphereical surface of radius equal to the range of the subsurface station. The seismic energies of the pulses recorded at the two stations were within 25 percent of each other which was within the accuracy of the data.

To compare the waveforms further, frequency analyses of the two signals were performed using the digital Fourier transform described in Appendix I. The fundamental period and time increment used were 5.0 seconds and 0.004 seconds, respectively. The spectral amplitudes to 25 cps are shown in Figure 7c, and the amplitudes for all frequencies less than eight cps are within 10 percent

for the two spectra. The amplitudes of frequencies above eight cps at station 2 were greater than those at station 3. Also, the spectrum of the signal at station 2 had secondary maxima centered about 11 and 17 cps which were not as evident in the spectrum of the signal at station 3. However, the differences in the spectra at the high frequencies were not considered significant to this research.

The spectral distribution of the seismic energy measured at each of the two recording stations was calculated using equation (19).

$$E(f_K) = 8\pi R^2 \rho c \Delta f \sum_{i=1}^{K} \left| G(f_i) \right|^2, \qquad (19)$$

where: R = the range of the subsurface station;

ρ = the density of the medium = 2.7 gm/cm^3;

c = the P wave propagational velocity of the medium = 5.1 km/sec;

Δf = the frequency increment = 0.2 cps; and

$\left| G(f) \right|$ = the modulus of the Fourier transform of the particle velocity waveforms.

The energies of the waveforms recorded at the two stations were within 25 percent of each other for frequencies $f \leq 25$ cps and within 20 percent for frequencies $f \leq 8$ cps.

It was concluded that, within the accuracy of the data, the particle velocity waveforms recorded at shot depth near the Hardhat explosion (granite medium) were indicative of the seismic signals that leave the explosions at various angles with the horizontal. However, the near-source recordings may not be as consistent for explosions located in other materials, such as alluvium or tuff. No data were available to determine the effects of inhomogenities of the near-source materials on the consistency of the subsurface recordings.

Since the explosions were located in the proximity of a free surface, the subsurface recordings may contain secondary arrivals such as reflections from the free surface. If a pure signal is contaminated by a secondary arrival, its spectrum will be modulated by a term which is dependent upon the relative amplitudes of the first and secondary arrivals and the time delay between them as shown in equation (20).

$$\left|S(w)\right| = \left|F(w)\right| \cdot \left[A^2+B^2+2AB\cos w\lambda\right]^{\frac{1}{2}}, \qquad (20)$$

where: $\left|S(w)\right|$ = the modulus of the composite signal;

$\left|F(w)\right|$ = the modulus of the uncontaminated signal;

A = the amplitude of the uncontaminated signal;

B = the amplitude of the secondary arrival;

λ = the time delay of the secondary arrival;

and

w = frequency in radians per second.

If B is small relative to A, the amplitude of the modulation term (the term within the brackets in equation (20) will approach A, the amplitude of the uncontaminated signal. The time delay, λ, governs the shape of the modulation term. The smaller the time delay, the broader the modulation term will be on the frequency axis (see Appendix II, Figure 20a). This modulation effect may be seen in Figure 7c, and the small amplitude secondary arrivals causing the modulation are indicated in the waveforms in Figure 7b by the arrows. The origin of the secondary arrivals is unknown. If the secondary arrivals were surface reflections, the propagation velocity of the arrivals would be approximately 6.6 km/sec as compared to the 5.1 km/sec propagation velocity observed for the first arrival. Further, the polarity of the secondary arrivals is opposite to that expected for compressional waves reflected from the free surface.

The amplitudes of the reflected compressional and the converted shear waves from the surface at the subsurface

stations were found to be less than ten percent of the amplitudes of the direct arrivals (Trembly, 1966). This resulted from the combined effects of the reflection coefficients, geometrical spreading, and attenuation losses over the additional path length. Hence, no corrections were made to the near-source waveforms to account for reflections from the free surface. However, the surface reflections may be important at greater epicentral distances and are considered later in this context. The effects of surface reflections on output signals are analyzed in detail in Appendix II.

Trembly and Berg (1966) compared the near-source seismic waves of the Hardhat, Haymaker and Shoal explosions to the signals from a theoretical point source described by Berg and Papageorge (1964). This comparison confirmed that the theoretical model provided a fair approximation to the P waves generated by explosions. These authors indicated that a component of the total amplitude of the theoretical signal decreased as the inverse square of the distance from the source; while the amplitude that propagated to large ranges decreased as the inverse distance (neglecting other losses) and it was termed the radiation field. The radiation field

component was determined for each of the particle velocity waveforms recorded at the near-source subsurface stations, and it was considered as the source function of the earth-receiver system.

Werth and Herbst (1962) defined the particle displacement in terms of a reduced displacement potential as shown in equation (21).

$$x(r,\tau) = -\frac{\partial}{\partial r}\left(\frac{\phi(\tau)}{r}\right), \tag{21}$$

where: $x(r,\tau)$ = particle displacement;

$\phi(\tau)$ = displacement potential;

τ = reduced time;

c = compressional wave propagation velocity;

and

r = range.

The particle velocity $u(r,\tau)$ would then be given by

$$u(r,\tau) = \frac{\phi'(\tau)}{r^2} + \frac{\phi''(\tau)}{rc}, \tag{22}$$

where ϕ' and ϕ'' denote differentiation with respect to τ. Since the term $\frac{\phi'(\tau)}{r^2}$ becomes negligible for large values of r, the term $\frac{\phi''(\tau)}{rc}$ is the component of the source which governs the character of the seismic waves at large epicentral distances (Berg and Long, 1966). The term

$\frac{\phi''(\tau)}{rc}$ corresponds to the radiation field. Solving equation (22) for the radiation field yields

$$\frac{\phi''(\tau)}{rc} = u(\tau) - \frac{c}{r}\exp\left(\frac{-c\tau}{r}\right)\int_0^{\tau}\exp\left(\frac{c\tau}{r}\right)u(\tau)\,d\tau . \qquad (23)$$

Equation (23) was solved numerically to obtain the radiation field component for each explosion. The results are shown in Figure 8. While the amplitudes of the radiation field components of particle velocity were slightly less than the total field amplitudes (compare Figures 4 and 8a), the character of the waveforms was not changed appreciably.

The spectral amplitudes of the Hardhat total and radiation field source functions are shown in Figure 8b. The spectral amplitudes of the radiation field waveform were approximately 10, 50, and 90 percent of the total field amplitudes for frequencies 0.2, 1.0, and 4.0 cps, respectively, and for frequencies greater than six cps the spectral amplitudes were the same. Therefore, the effect of removing the term $\frac{\phi'(\tau)}{r^2}$ from the total field was to reduce the low frequency content of the source function. This effect was predictable since the operation defined by equation (23) removed any long-period or residual displacements from the total amplitudes of the source waveforms by making the net area under the particle

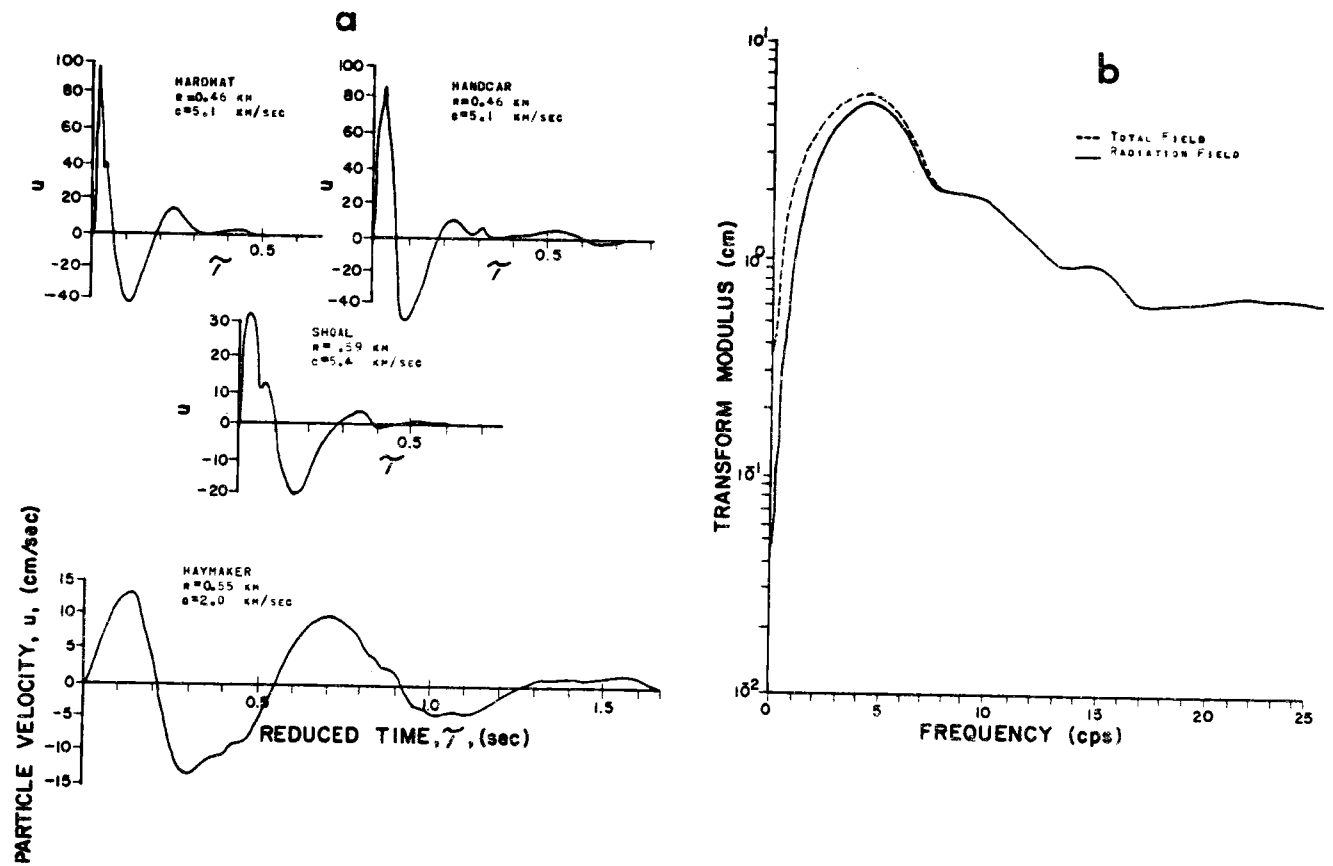

Figure 8a. Waveforms of the radiation fields of the observed source signals.

b. Comparison of the spectral amplitudes of the total and radiation fields for the source signal of the Hardhat nuclear explosion.

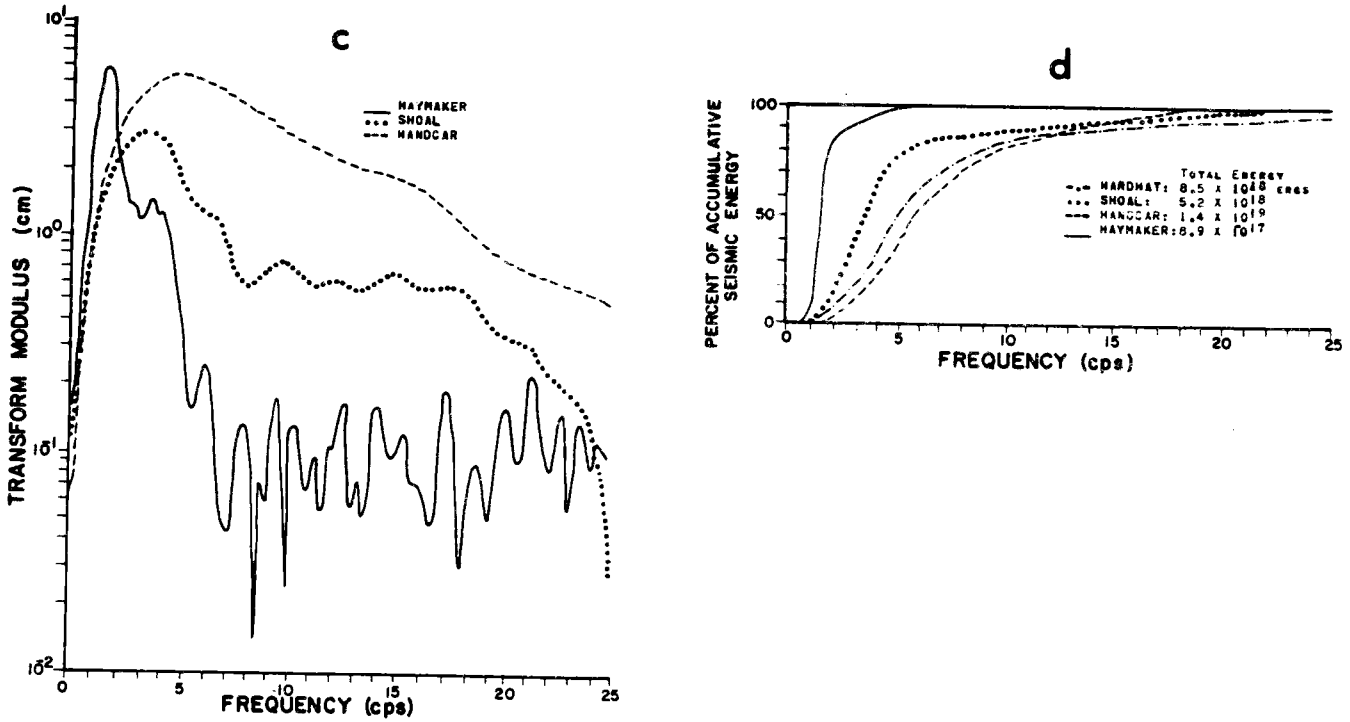

Figure 8c. Comparison of the spectral amplitudes of the radiation fields of the Haymaker, Shoal, and Handcar nuclear explosions.

d. Comparison of the spectral distribution of the seismic energy of the Hardhat, Haymaker, Shoal, and Handcar explosions.

velocity functions equal to zero.

The spectra of the radiation field of the source functions for the Haymaker, Shoal, and Handcar nuclear explosions are shown in Figure 8c. The Haymaker (alluvium) spectrum peaked at approximately 1.4 cps. Above five cps the spectral amplitudes were approximately two percent of the peak amplitude, and were not reliably related to the source. The spectra of the source functions for the explosions in granite (Hardhat, Shoal) and dolomite (Handcar) were broader than that in alluvium (Haymaker) due to the impulsive nature of the former sources. The Hardhat and Handcar spectra peaked at 4.4 cps and decreased slowly above six cps (4 decibels per octave). The Shoal spectrum peaked at 3.6 cps and decreased to approximately 20 percent of the peak amplitude at 18 cps. The spectral distribution of seismic energy of each of the source functions (radiation field) was calculated, and the percentage of the accumulated energy plotted versus frequency is shown in Figure 8d for each of the sources. The total seismic energy of each of the source functions (see equation (18)) is also given in the figure. Eighty percent of the P wave seismic energy was contributed by frequencies in the band $1 \leqslant f \leqslant 3$ cps for Haymaker,

$2 \leqslant f \leqslant 8$ cps for Shoal, and $3 \leqslant f \leqslant 12$ cps for Hardhat and Handcar. Although the seismic energies of the Hardhat and Handcar sources were approximately one order of magnitude greater than that of the Haymaker source, only ten percent of the Hardhat and Handcar energies were concentrated in the frequencies less than three cps. Therefore, all of the seismic source energies were approximately equal for those frequencies ($0.2 \leqslant f \leqslant 3$ cps). These differences in the spectral distribution of the seismic energies for the different sources may partially reflect the effects of attenuation of the energy due to propagation of the signals to the subsurface stations. The extent to which this is the case is not known, and the effect is assumed to be negligible.

Synthesized primary waves

The first motions on the records shown in Figure 6 include the primary waves from the explosions as well as any reflections from the free surface and other later pulses. The beginnings of the primary waves were well defined, but the duration of the pulses were, in some cases, difficult to determine due to the complexity of the observed records. The source functions shown in

Figure 8 were used to synthesize distant signals to aid in determining the duration of the observed primary wave at each station. The initial waves were synthesized by operating on the source functions with a mathematical attenuation filter and an instrument response operator applicable for each recording station. The effects on distant signals of the surface reflection from the source were considered because the reflected signal may alter the primary wave that was received.

Neglecting boundary losses, geometrical spreading, and crustal effects at the receiver, the spectrum of the signal at a recording station is related to the input source signal as shown in equations (24) and (25).

$$\left|F_{out}(w)\right| = \left|A(w)\right| \left|I(w)\right| \left|F_{in}(w)\right| \tag{24}$$

$$\Theta_{out}(w) = \phi_A(w) + \phi_I(w) + \Theta_{in}(w), \tag{25}$$

where: $\left|F_{out}(w)\right| e^{i\Theta_{out}(w)}$ = Fourier transform of the received signal;

$\left|A(w)\right| e^{i\phi_A(w)}$ = attenuation operator;

$\left|I(w)\right| e^{i\phi_I(w)}$ = the recording instrument response; and

$\left|F_{in}(w)\right| \; e^{i\Theta_{in}(w)}$ = Fourier transform of the input source signal.

$\left|F_{out}(w)\right|$ and $\Theta_{out}(w)$ in equations (24) and (25) represent the modulus and phase of the signal at the station if no secondary arrivals are considered. If the source signal has been contaminated by a reflection from the free surface above the source, then the input signal will be a combination of the pure source signal and the reflected signal. It was assumed that the reflection coefficient for the free surface is not a function of frequency and is negative (i.e. a compressional wave reflected from a free surface is 180 degrees out-of-phase with the incident wave at the angles of incidence considered in this research). Equations (24) and (25) are then expressed in a form analogous to equation (20) (see Appendix II), as shown in equations (26) and (27).

$$\left|F_{out}(w)\right| = \left|A(w)\right| \left|I(w)\right| \left|F_{in}(w)\right| \left[1 + |R|^2 - 2|R| \cos(w\lambda)\right]^{\frac{1}{2}} \quad (26)$$

$$\Theta_{out}(w) = \phi_A(w) + \phi_I(w) + \tan^{-1}\left(\frac{|R| \sin(w\lambda)}{1 - |R| \cos(w\lambda)}\right), \quad (27)$$

where: $|R|$ = the reflection coefficient at the surface, $(0 \leq R \leq 1)$; and

λ = the delay time of the surface reflection.

When solving dynamic problems in seismology such as determining the seismic waveforms at various epicentral distances from an explosion, allowance must be made for the fact that the earth is not an ideal elastic medium. It is an absorbing and scattering medium in which part of the mechanical energy of the P waves is converted to other phases and to other forms of energy such as heat. Kogan (1966) has analyzed and summarized many of the suggested mathematical models for attenuation as to their success in describing the observed phenomena and in satisfying the basic requirements of the propagation of seismic waves. Although there is no general agreement on the best way to represent the attenuation of seismic wave energy, the attenuation filter suggested by Futterman (1962) has been used in studies involving seismic wave attenuation by several investigators. Werth, Herbst, and Springer (1962) and Werth and Herbst (1963) used this filter together with appropriate instrument responses and crustal models to synthesize the seismic waves recorded to epicentral distances of 600 kilometers from underground explosions. Wuenschel (1965) experimentally verified the attenuation filter using models to simulate real earth

materials. Laun (1965) used the attenuation filter in the reverse problem of describing the Gnome source function from recordings at epicentral distances from 250 to 350 kilometers. Carpenter (1966, 1967) used Futterman's attenuation filter together with appropriate receiver responses to synthesize the seismic waveforms recorded at teleseismic distances from underground, underwater, and atmospheric explosions.

In this research, Futterman's attenuation filter was used in the synthesis of the waveforms. For the frequencies considered ($0.2 \leq f \leq 25$ cps), the modulus of the attenuation filter, $|A(w)|$, and the accompanying phase relation, $\phi_A(w)$, necessary to satisfy the causality condition reduce to equations (28) and (29), respectively (Werth, Herbst, and Springer, 1962; Sarmah, 1966).

$$|A(w)| = \exp\left(\frac{-\pi T f}{Q}\right) \tag{28}$$

$$\phi_A(w) = \left\{1 - \frac{\mathrm{Ln}(f_o/f) - (\mathrm{Ln}\gamma)}{\pi Q}\right\} 2\pi f T, \tag{29}$$

where: $|A(w)|$ = modulus of the filter;

$\phi_A(w)$ = phase of the filter;

w = frequency in radians per second;

f = frequency in cycles per second (cps) = $\frac{w}{2\pi}$;

f_o = cutoff frequency = $\Delta f/20$;

Δf = fundamental frequency = 0.2 cps;

T = traveltime (r/c);

c = propagation velocity;

r = epicentral distance;

$\text{Ln}\,\gamma$ = 0.5772157 = Euler's constant; and

1/Q = specific dissipation function.

The attenuation filter, A(w), applicable for each recording station was calculated from equations (28) and (29) using traveltimes from Table II and values of Q given by Sarmah (1966) and Long (1967)[6]. The moduli of the attenuation filters used, the LRSM instrument velocity sensitivity, the Handcar source spectrum, and the surface reflection modulator for $|R|$ = 1.00 and λ = 0.2 seconds are shown in Figure 9a. (The arrows in the troughs indicate that the amplitudes of the modulation term go to zero, which is only the case when $|R|$ = 1.00). The spectra synthesized for stations MN-NV, UBSO, and MBC using the Handcar source are shown in Figure 9b. The

6. Long, L.T. 1967. Assistant in Oceanography, Oregon State University, Department of Oceanography. Personal communication. Alexandria, Virginia.

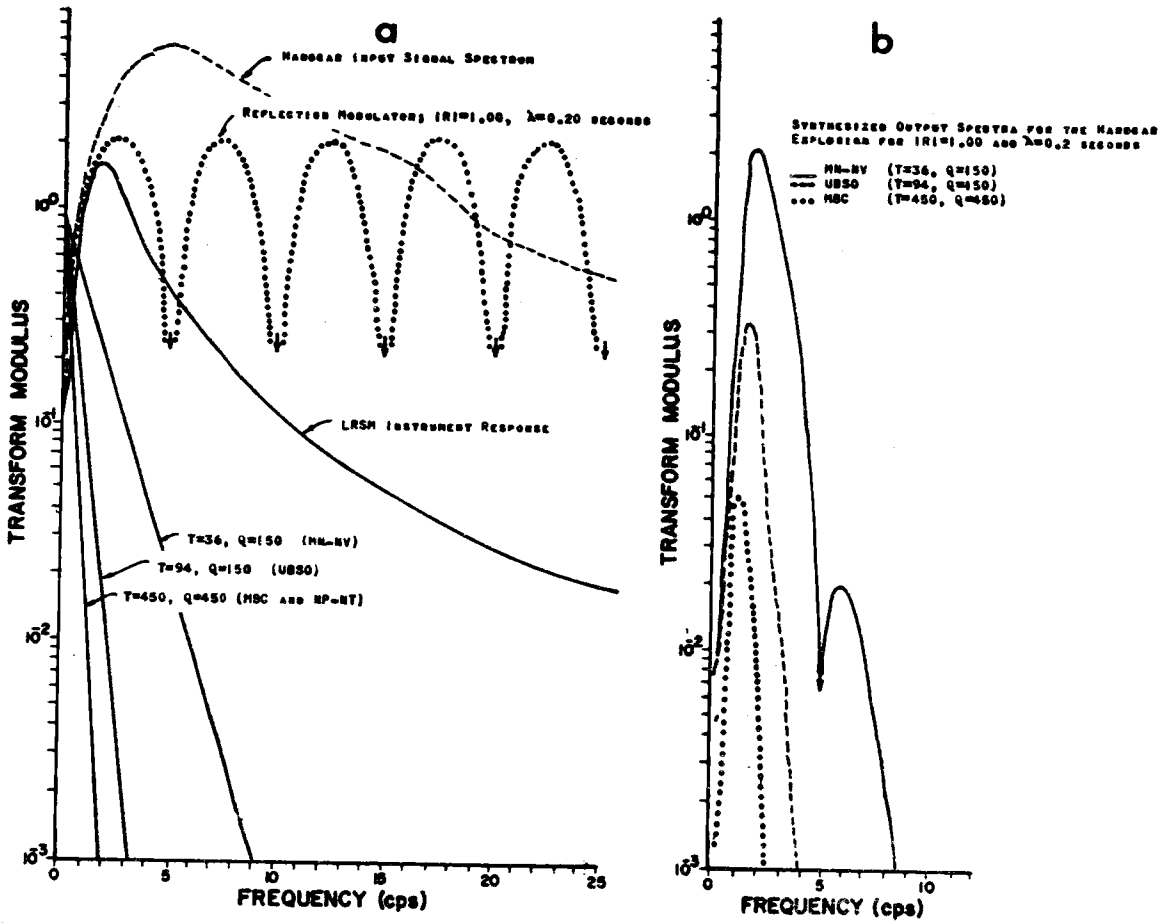

Figure 9. (a) The spectral amplitudes of the Handcar source signal LRSM instrument response, attenuation filters, and the surface reflection modulator for $|R| = 1.00$ and $\lambda = 0.20$ seconds.
(b) Synthesized spectral amplitudes using the Handcar source signal for stations MN-NV, UBSO, and MBC.

amplitudes of the synthesized spectra were limited on the high-frequency end of the passband by the attenuation filters. On the low-frequency end the spectra were limited by the small number of low frequencies present in the source functions and by the lack of response of the recording systems to the low frequencies. Also, the effect of the surface reflection modulator on the synthesized spectra was small due to the dominant effect of the attenuation filters on the shape of the synthesized spectra at the high frequencies.

The synthesized pulses were formed from the synthesized spectra using the digital inverse Fourier transform with a fundamental period of five seconds. The pulses synthesized for stations MN-NV, UBSO, and MBC using the Handcar and Haymaker sources with no surface reflections included (R = 0) are compared to each other and to be observed signals in Figure 10a. Since boundary losses and geometrical attenuation were not included in the synthesis, the absolute amplitudes of the distant signal were not known. For this reason, the amplitudes of the first half-cycle of the synthesized and observed signals were normalized. A detailed analysis of the observed signals is presented later in this chapter, but

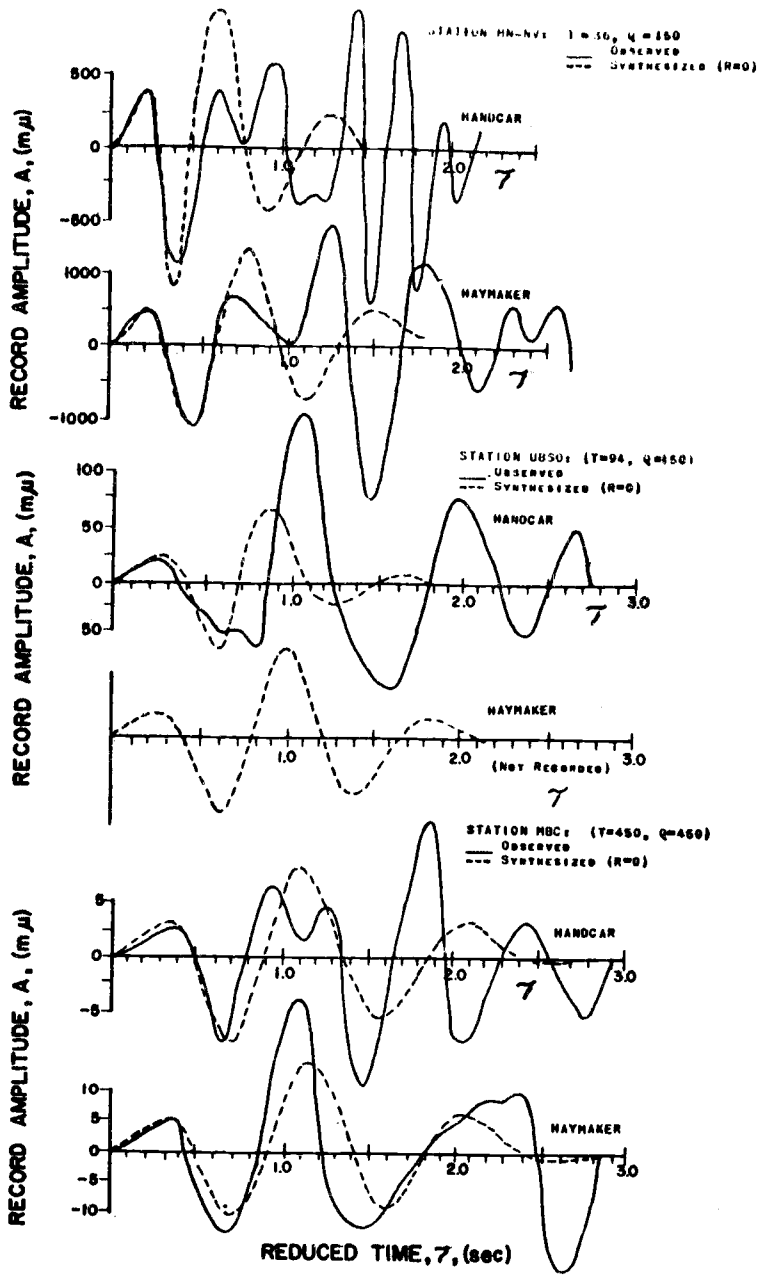

Figure 10a. Comparison of the primary waves synthesized using the Handcar and Haymaker source signals and the signals observed at stations MN-NV, UBSO, and MBC from those explosions.

A = normalized record amplitude in millimicrons (mμ).

τ = reduced time in seconds.

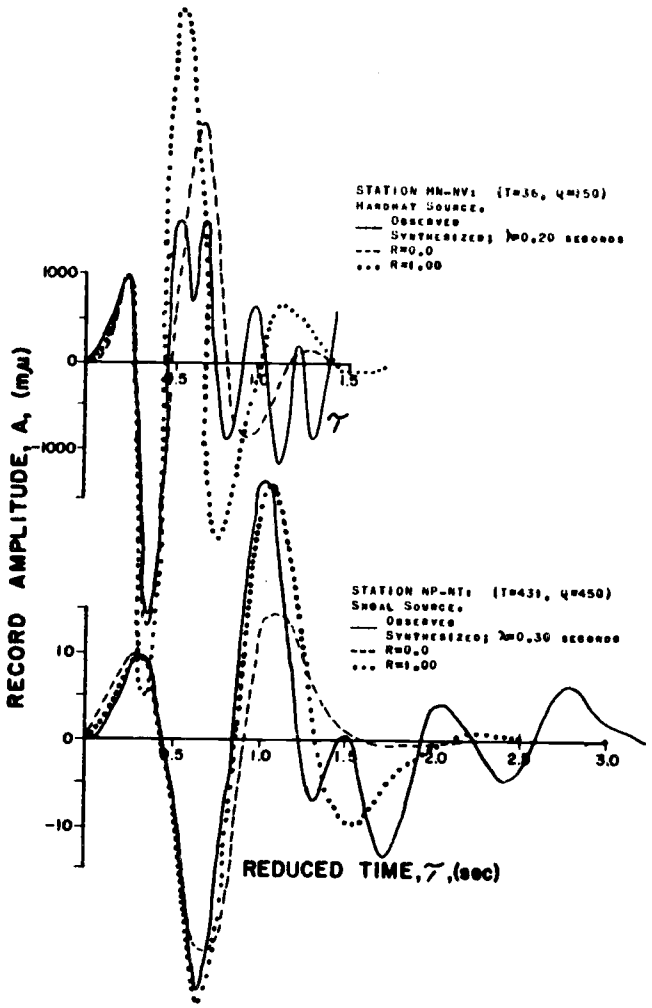

Figure 10b. Effect of surface reflections on the comparison of the observed and synthesized signals for the Hardhat (MN-NV) and Shoal (NP-NT) source signals.

A = normalized record amplitude in millimicrons (mμ).

τ = reduced time in seconds.

a cursory comparison between the observed and derived signals is given below.

At station MN-NV, the pulse synthesized using the Handcar source was shorter in time duration than that synthesized using the Haymaker source. This was due to the high-frequency content of the Handcar source function as compared to that of the Haymaker source. However, as the epicentral distance was increased, the signals synthesized using source signals from different explosions became more nearly similar in duration and waveform due to the attenuation of the high frequencies. At the greater epicentral distances, the low-frequency portion of the source spectra governed the character of the synthesized waveforms. Since all of the source spectra were very similar for the low frequencies (see Figure 8c), the synthesized waveforms were similar.

At station MN-NV, the observed Handcar and Haymaker signals were similar to the synthesized signals for the first cycle. After the first cycle, the observed signals were contaminated by secondary arrivals and were not similar to the synthesized signals. At station UBSO, the observed signal from the Handcar source was evidently contaminated by other arrivals in the initial portion of

the signal and did not compare well with the synthesized signals. At station MBC, the Handcar signal was contaminated by a large amplitude secondary arrival at approximately 1.1 second and was similar to the synthesized signal for the first cycle of motion only. Although the third half-cycle of the observed signal at MBC from the Haymaker source had a larger amplitude than that of the synthesized signal, the two waveforms were similar until 2.4 seconds when a secondary arrival was evident in the observed signal.

In Figure 10b the observed signals for station MN-NV (Hardhat) and NP-NT (Shoal) are compared to the waveforms synthesized with no surface reflection of energy ($|R| = 0$) and to the waveforms synthesized with a total surface reflection of energy ($|R| = 1.00$).[7] At station MN-NV, the first cycle of the pulse synthesized with no surface reflection closely approximated the first cycle of the

7. The delay times were approximated using the propagational velocities observed at the subsurface stations and the depths of the explosions given in Table I. Several values of R between zero and one were used in the synthesis, but only the waveforms calculated using the extreme values ($|R| = 1.00$ and $|R| = 0$) are shown in Figure 10b.

observed signal, whereas the waveform synthesized with the included surface reflection was a poorer approximation to the observed signal. After the first cycle the observed signal was contaminated by other arrivals of seismic energy and was not similar to either of the synthesized pulses. At station NP-NT, the amplitudes of the first three half-cycles of the observed signal (Shoal) were closely approximated by the waveform synthesized with the surface reflection included, whereas the amplitudes of the second and third half-cycles of the synthesized pulse were too small when no surface reflection was included. Additional contamination of the observed signal by arrivals after approximately 1.3 seconds precluded comparison of the synthesized and observed signals after that time.

Although the addition of a surface reflection improved the comparison of the synthesized pulses to the observed waveforms in some instances, this was not always the case, and no conclusion as to the presence of the reflection could be made from these data. The purpose of synthesizing the waveform was to help determine the character and duration of the primary waves (first arrivals) recorded at distant stations. Thus, the

synthesized arrivals would serve as an aid in picking the signals to be used in later analysis. It was found that while the character of the pulse was affected by surface reflections, the time durations of the synthesized pulses were not affected. This was due to the fact that the attenuation filters dominated the synthesized spectra, and the modulation effect of the surface reflection was superimposed on the rapidly decreasing spectral amplitudes (see Figure 9b). Therefore, the reflections did not appreciably modify the duration of the synthesized waveforms. The derivation of the source characteristics from a distant signal which is complicated by a surface reflection is discussed briefly in the next section and in greater detail in Appendix II.

Derived source functions

In this section the seismic signals recorded at near-regional, regional, and teleseismic distances (see Figure 6) are Fourier analyzed, and the effects of secondary arrivals and noise on the spectra are discussed. A near-source signal from an explosion is used with signals from the explosion recorded at the different epicentral distances to calibrate the stations. Source signals for

other explosions are derived using distant signals recorded from them with the method defined by equations (15), (16), and (17). The derived source signals are compared to those observed near the explosions as to waveform, spectral content, and energy content. The effects of each of the constraints discussed earlier (see Chapter I, page 14-16) are described. The analyses are presented separately for the near-regional, regional, and teleseismic distances.

Near-regional distance. - The seismic signals recorded at station MN-NV were shown in Figure 6a, and the synthesized signals for that station (Hardhat, Handcar, and Haymaker sources) were shown in Figure 10. The synthesized signals were between 1.0 and 1.5 seconds duration, depending upon the impulsiveness of the source function used in the synthesis. The observed waveforms were similar to the synthesized signals for the first cycle of motion, which was approximately 0.5 seconds of record (see Figure 10). After the first cycle, the observed waveforms were contaminated by other waves arriving at the station. At station MN-NV, a prominent arrival was recorded approximately 1.2 seconds after the time of the first arrival (initial motion at $\tau = 0$,

reduced time), and another large amplitude phase arrived at approximately 2.5 seconds.

The arrival at 1.2 seconds made it necessary either to truncate the recordings at or less than one second, or to include that arrival and truncate the records before the next arrival at 2.5 seconds. In order to examine all possibilities, the Hardhat recording was truncated at 0.6, 1.0, and 2.2 seconds, and each signal was transformed into the frequency domain. The Fourier amplitude spectra are shown in Figure 11a. The fundamental period and time increment used in the digital Fourier transform (see equations (32) and (33) in Appendix I) were 5.0 and 0.02 seconds, respectively. The arrows shown with the signal in the figure indicate the truncation times. The amplitudes of the spectra were normalized to the peak amplitudes for comparison purposes, and the actual amplitude of the peak of each spectrum (Am) is given in the figure. The spectrum of each truncated pulse peaked at 2.4 cps and decreased rapidly to ten percent of the peak amplitude by six cps and to approximately two percent of the peak amplitude by eight cps. At frequencies greater than ten cps the amplitudes were approximately one percent of the peak amplitude.

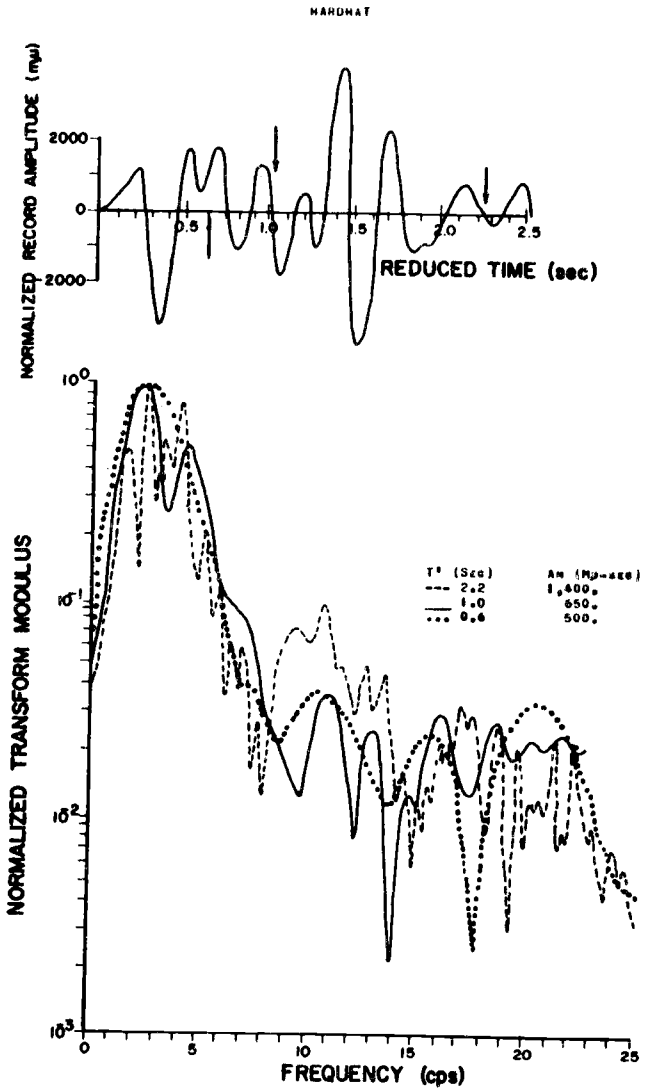

Figure 11a. Output signals at station MN-NV and the spectral amplitudes for the Hardhat nuclear explosion.

T' = time duration of the output signal used.

Am = the amplitudes of the peak of each spectrum.

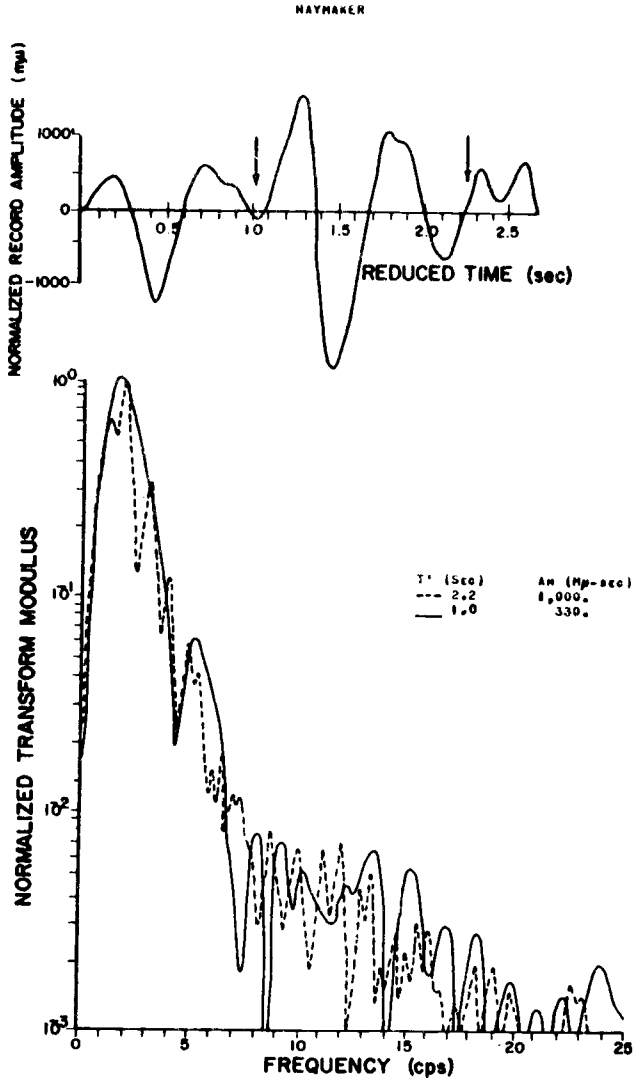

Figure 11b. Output signals at station MN-NV and the spectral amplitudes for the Haymaker nuclear explosion.

T' = time duration of the output signal used.

Am = the amplitudes of the peak of each spectrum.

The spectrum of the signal truncated at 2.2 seconds varied rapidly, partially due to the modulating effect of the secondary arrival at 1.2 seconds (see equation (20)). The spectrum of the signal truncated at one second was smoother but had a second maximum centered at about 4.2 cps, partially due to the modulating effect of the four cps rider included in the signal (see the signal in Figure 11a). The spectrum of the signal truncated at 0.6 second was smoother than the other spectra and showed no modulation effects for frequencies below eight cps. The spectra were smoother as the duration of the signal was decreased due to a combination of the removal of secondary arrivals and to the decreased frequency resolution according to the uncertainty principle associated with the Fourier transforms (Papoulis, 1962; Huang, 1966).

The amplitudes of the spectra of the Haymaker signal which was truncated at 1.0 and 2.2 seconds are compared in Figure 11b. The spectrum of the 1.0 second duration signal was smoother than the spectrum of the 2.2 second signal. Each of the Haymaker spectra peaked at 1.6 cps as compared to 2.4 cps for the Hardhat spectra. The amplitudes decreased to ten percent of the peak amplitudes by four cps and to one percent by seven cps.

The spectral amplitudes of the Bilby, Handcar, and Pile Driver recordings truncated at approximately one second are compared in Figure 12 for station MN-NV. Each spectrum is normalized to its peak amplitude. The spectra were similar below eight cps in that they all peaked at approximately 2 cps and decreased to ten percent of the peak amplitude by four cps. However, the frequency and amplitude of the secondary maxima and the character of each spectrum above eight cps differed for each signal. The amplitudes of the Hardhat and Handcar spectra (not shown in Figure 12) were approximately ten times greater than the amplitudes of the Haymaker, Bilby, and Pile Driver spectra at frequencies above ten cps, due to the different digitizing procedures used (see the discussion in Chapter II), but the effect was outside the band of frequencies for which the instruments were reliably calibrated.

If the passbands of reliable frequencies of the spectra are defined as those frequencies for which the amplitudes are greater than ten percent of the peak amplitudes, then the low-frequency cutoff was 0.2 cps and the high-frequency cutoff was 4.0 cps for all of the output signal spectra at station MN-NV. If the spectral

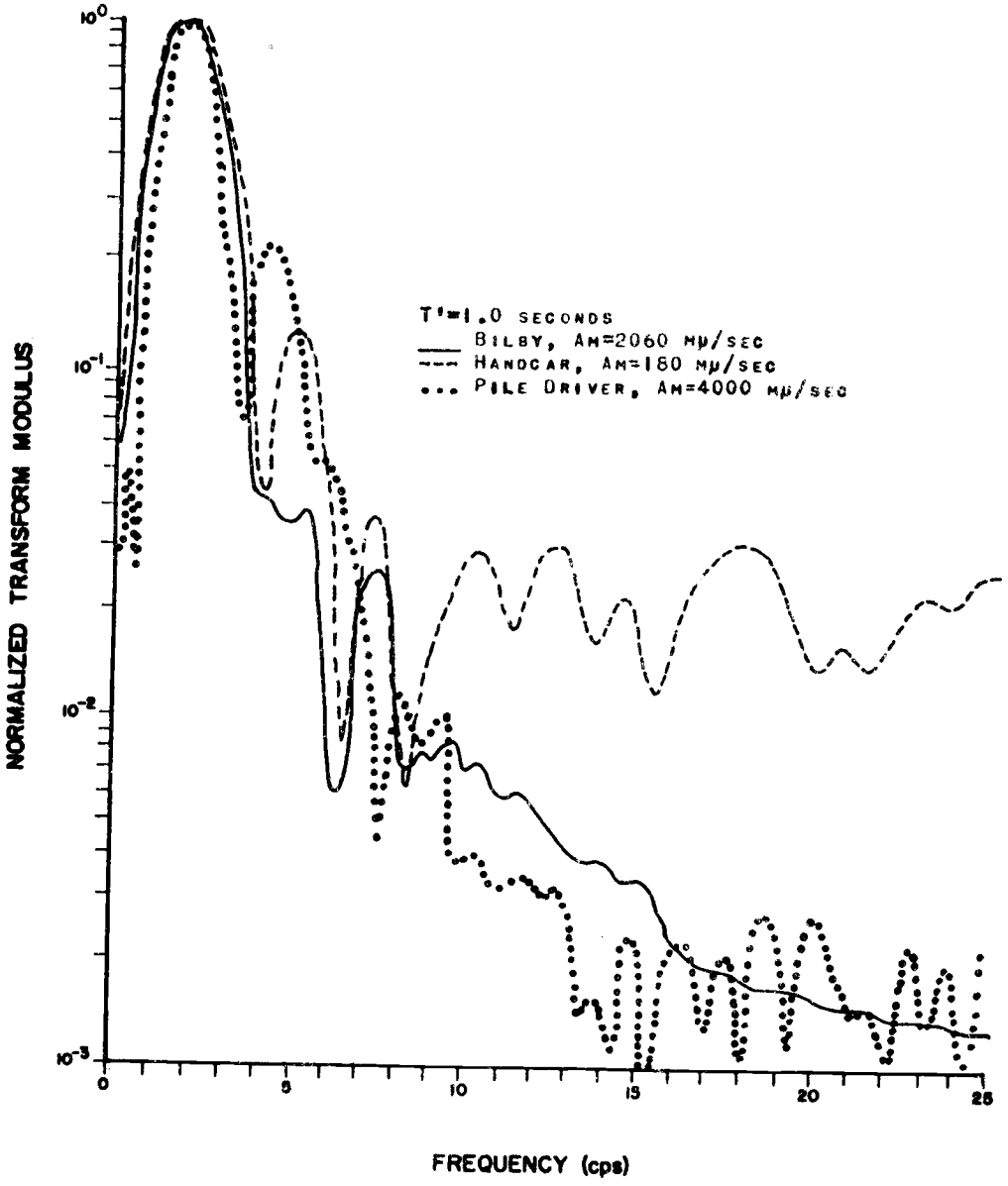

Figure 12. Spectral amplitudes of signals at station MN-NV from the Bilby, Handcar, and Pile Driver nuclear explosions.
T' = duration of the output signals used.
Am = the amplitude of the peak of each spectrum.

amplitudes above ten cps are assumed to be dominated by noise, then the above definition of the most reliable frequencies is equivalent to a minimum allowable signal-to-noise ratio of 10/1 in the spectra.

It was shown in equation (26) that the effect of contaminating an output signal with a reflection, from the free surface near the source, would be to modulate the output signal spectrum. However, for the synthesized output spectra of distant signals, the modulation effect was not pronounced because the spectral amplitudes decreased rapidly at the high frequencies due to the effects of attenuation (see Figure 10b). The modulation effect of surface reflections possibly contained in the spectra of output signals shown in Figures 11 and 12 was not clearly evident. The combination of the effects of attenuation and of modulation of the spectra by other secondary arrivals, for which the delay times and amplitudes were greater than those of possible surface reflections, would have masked any modulation by surface reflections. When the time duration of the output signals was decreased to remove the effects of other secondary arrivals, no modulation was observed in the spectra of the output signals within the passbands of reliable frequencies. Therefore,

no conclusions could be drawn from these data as to whether surface reflections contaminated the first arrivals at the station MN-NV.

The criteria for selecting an explosion (source) to calibrate the earth-receiver system are: (1) the source function must be known; (2) the source function should be impulsive to allow the station to be calibrated for as many frequencies as possible; and (3) the signal level at the station of interest should be large in order to minimize the effects of noise. (Noise was defined as any portion of the signal which is not source-related). Calibration sources which satisfy these criteria make it possible to determine the limitations imposed on the method by the constraints discussed on pages 14-16 in Chapter I.

On the basis of the above criteria the Hardhat explosion was used to calibrate the station MN-NV for seismic signals from nuclear explosions in the Nevada Test Site. Equations (15) and (16) were used to derive the spectra of the source functions for events, other than the Hardhat explosion, which are listed in Table II. In equations (15) and (16) $\left|C_{in}(w)\right| e^{i\Theta_{in}(w)}$ and $\left|C_{out}(w)\right| e^{i\Theta_{out}(w)}$ were the spectra of the observed Hardhat source function and output signal, respectively,

and $|U_{out}(w)| \quad e^{i\Psi_{out}(w)}$ was the spectrum of the output signal of the event for which the source function was to be derived.

The moduli of the source spectra derived for Haymaker using the output signals truncated at 2.2 and 1.0 seconds are compared to the observed source spectrum in Figure 13a for frequencies to the folding frequency of the data (25 cps).[8] The source spectrum derived using the 2.2 seconds duration output signals was rapidly varying even within the passband of reliable frequencies ($f \leqslant 4$ cps). This was due to the modulating effects of a large amplitude secondary arrival at 1.2 seconds in the output signal (see Figure 6a) for which the calibration was evidently not adequate. It is shown in Appendix II that if the calibration does not include the effects of a secondary arrival adequately (both in character and arrival time), then spikes may appear in the derived source spectra - as was the case here.

The Haymaker source spectrum derived using the 1.0

8. The analysis was also carried out using the Hardhat output signal truncated at 0.6 seconds, but the results did not differ significantly from those obtained using the signal truncated at one second.

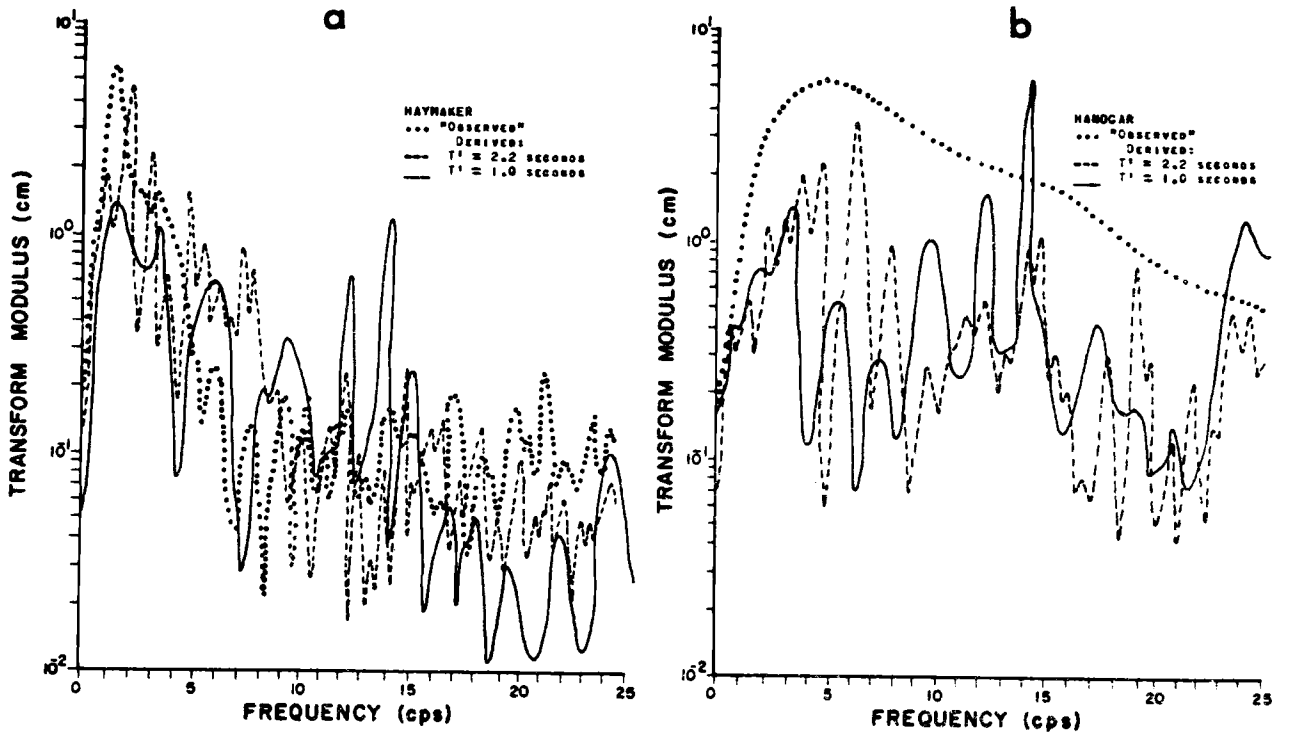

Figure 13. Comparison of the "observed" and derived source spectra for the (a) Haymaker and (b) Handcar nuclear explosions. Station MN-NV - Hardhat calibration.
T' = the time duration of the output signals used.

second duration output signals was smoother than the above spectrum but had less amplitude than the "observed" source spectrum ($f \leq 4$ cps). The derived spectrum contained large amplitude spikes at frequencies about four cps which were due to the effects of noise in the two (Hardhat and Haymaker) output spectra (see equation (15) and Figure 11).

The amplitudes of the source spectra derived for the Handcar explosion using output signals truncated at 2.2 and 1.0 seconds are compared to the "observed" Handcar source spectrum in Figure 13b for frequencies to the folding frequency (25 cps). The source spectra derived using the 1.0 and 2.2 seconds duration output signals were somewhat similar to the "observed" Handcar spectrum for frequencies less than four cps. At frequencies above four cps the derived spectra had isolated large amplitude spikes due to the output signal spectra having been dominated by noise at those frequencies. At all frequencies the derived spectral amplitudes were less than those of the "observed" spectrum.

The source functions, $u_{in}(t)$, for both of the derived source spectra (one and 2.2 second signals) for the Haymaker explosion were obtained using the inverse

Fourier transform and using: (1) all frequencies to the folding frequency ($f \leqslant 25$ cps) and (2) only the reliable frequencies ($f \leqslant 4$ cps) are shown in Figure 14a. The observed source function for the Haymaker explosion is shown in the figure for comparison with the derived functions. It should be noted that filtering the frequencies above four cps from the observed source function did not significantly alter the character of the waveform because the amplitudes for these frequencies were negligibly small (see Figure 8c).

The source functions obtained from the spectra derived using the 2.2 second duration output signals were essentially two cps sine waves oscillating over the complete fundamental period because the spike at two cps in the derived spectrum was dominant. The spike was a consequence of the secondary arrival at 1.2 seconds in the Hardhat and Haymaker output signals at MN-NV, which was apparently not as profound in the Hardhat data, and was not incorporated into the calibration sufficiently.

The source function obtained from the spectra derived using the 1.0 second duration output signals was similar in waveform to the observed source function when only the reliable frequencies were used. However, the

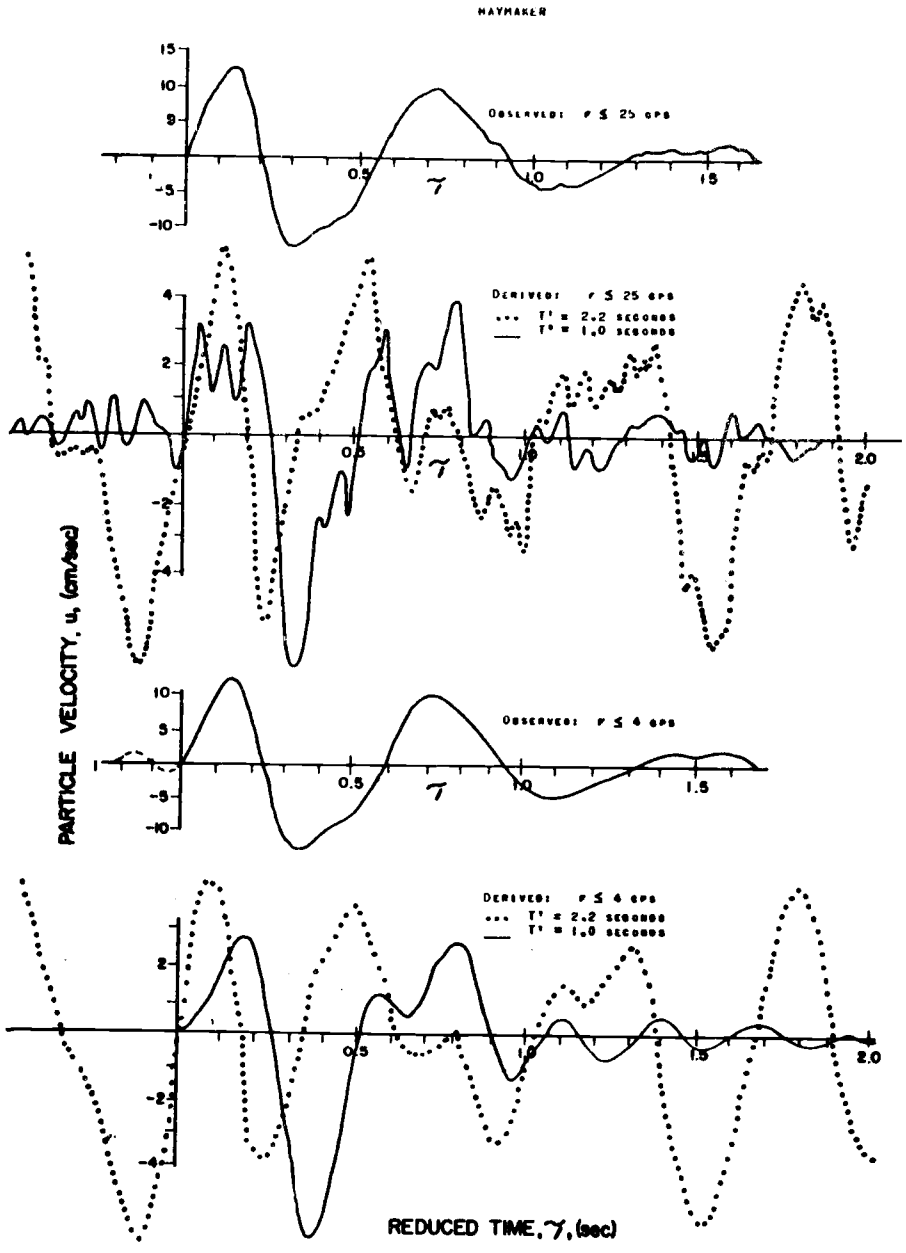

Figure 14a. Comparison of the observed and derived source signals for the Haymaker nuclear explosion, station MN-NV - Hardhat calibration.

T' = time duration of the output signals used.

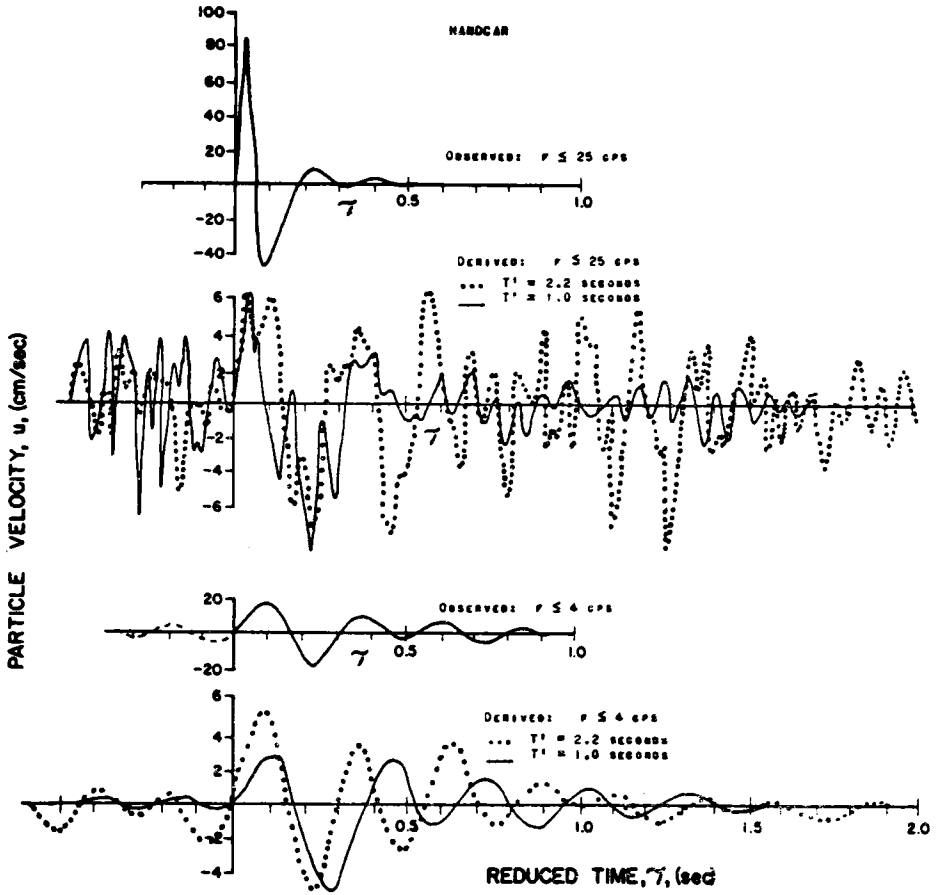

Figure 14b. Comparison of the observed and derived source signals for the Handcar nuclear explosion, Station MN-NV - Hardhat calibration

T' = time duration of the output signals used.

amplitude of this derived source function was only 30 percent of the amplitude of the observed source function.

The source functions obtained for the Handcar explosion using both the derived source spectra are compared to the observed source function in Figure 14b, for $f \leqslant 25$ cps and $f \leqslant 4$ cps.[9] The source function calculated using all of the frequencies was very oscillatory due to the large amplitude spikes in the derived source spectra for frequencies greater than four cps. When only the frequencies less than four cps were used, both of the derived source functions were similar in character to the observed source function but were only ten percent of the amplitude of it.

The seismic energies of the derived sources for the Haymaker, Bilby, Handcar, and Pile Driver explosions were calculated (see equation 19) from the derived source spectra and are given in Table III. The frequency bands used in the calculation of energy were $f \leqslant 4$ cps (the band of reliable frequencies), and $f \leqslant 25$ cps (the total band of frequencies to the folding frequency of the data). The density, P wave propagational velocity, and range used in

9. The precursor shown in the observed source function for $f \leqslant 4$ cps was due to the ideal low-pass filter used, which is noncausal.

TABLE III. Comparison of seismic energies of "observed" and derived sources (MN-NV)-Hardhat calibration).

Explosion	Frequencies used (cps)	"Observed" source energy ($\times 10^{18}$ ergs)	Source energy computed using signals of duration: 2.2 seconds ($\times 10^{18}$ ergs)	1.0 second ($\times 10^{18}$ ergs)
Haymaker	$f \leq 25$	0.89	2.5	0.81
	$f \leq 4$	0.82	1.9	0.58
Bilby	$f \leq 25$		320.	52.
	$f \leq 4$	42. *	250.	37.
Handcar	$f \leq 25$	14.	2.0	1.4
	$f \leq 4$	3.2	0.46	0.22
Pile Driver	$f \leq 25$	**	48.	70.
	$f \leq 4$		32.	42.

* Estimated from close-in surface measurements (Sarmah, 1966).
** No information available.

the calculations to the Hardhat source (the method used to derive the spectra assumed these parameters to be the same for the unknown sources as for the calibration source). The energies of the observed sources for the Haymaker and Handcar explosions are also given in the table for the corresponding frequencies and the known parameters of the sources. No subsurface instruments recorded source signals from the Bilby or Pile Driver explosions. However, the seismic energy from the Bilby explosion was estimated by Sarmah (1966) using strong-motion surface instruments located from three to eighteen kilometers from the source.

The energies computed using all frequencies ($f \leqslant 25$ cps) are shown only for comparison and are not reliable due to the predominance of noise in the output spectra. The effect of the secondary arrivals in the output signals of 2.2 seconds duration was to increase the derived source energies for all of the explosions except Pile Driver, and this effect was most pronounced for the Bilby explosion. From considerations of the output signal spectra, the characteristics of the derived sources, and the synthesized output signals, the most reliable energies of the derived sources were those computed using the 1.0 second duration output signals for frequencies less than

4 cps (see the underlined values in Table III). The energies of the derived sources for the Haymaker, Bilby and Handcar explosions were 70, 90, and 7 percent of the observed source energies, respectively. The small percentage for the Handcar source was due to the small amplitudes of the Handcar signal at station MN-NV. This phenomenon will be discussed later in conjunction with the results using data from more distant recording stations.

The source energy derived for the Pile Driver explosion did not vary greatly with the duration of the output signals (for the reliable frequencies). This explosion was detonated in the same location as the Hardhat explosion (see Table I). Therefore, this consistency of the energies of the derived sources may reflect a higher degree of reliability for the calibration made using input and output signals from the Hardhat explosion. However, since subsurface data were not available for the Pile Driver explosion, no estimate of the accuracy of these results can be made.

Regional distance. - Approximately four seconds of the initial P waves recorded at station UBSO were shown in Figure 6b. The observed signals from the explosions

in the Nevada Test Site (Bilby, Handcar, and Pile Driver) were characterized by first cycles of small amplitude and second cycles of relatively large amplitude. In this respect, the arrivals were not similar to the synthesized signals, which were shown in Figure 10a. The observed signal recorded at UBSO from the Shoal explosion was complicated by several large-amplitude secondary arrivals, the first occurring at one second and another at two seconds after the onset of the first arrival. The differences in the character of the signal from the Shoal explosion (central Nevada) and those from the explosions in the Nevada Test Site were, presumably, due to the differences in the propagation paths from the explosions to the station (see Figure 3a). The signal from the Shoal explosion and those from the Nevada Test Site were analyzed to determine the effects of differences in the propagation paths on the calibration method used in this research. For these explosions, the epicentral distances were approximately the same (see Table II and Figure 3a).

The observed signal from the Handcar explosion was truncated at 1.3 and 2.2 seconds, and the amplitudes of the Fourier spectra for the truncated signals are shown in Figure 15a. The signal from Handcar was truncated

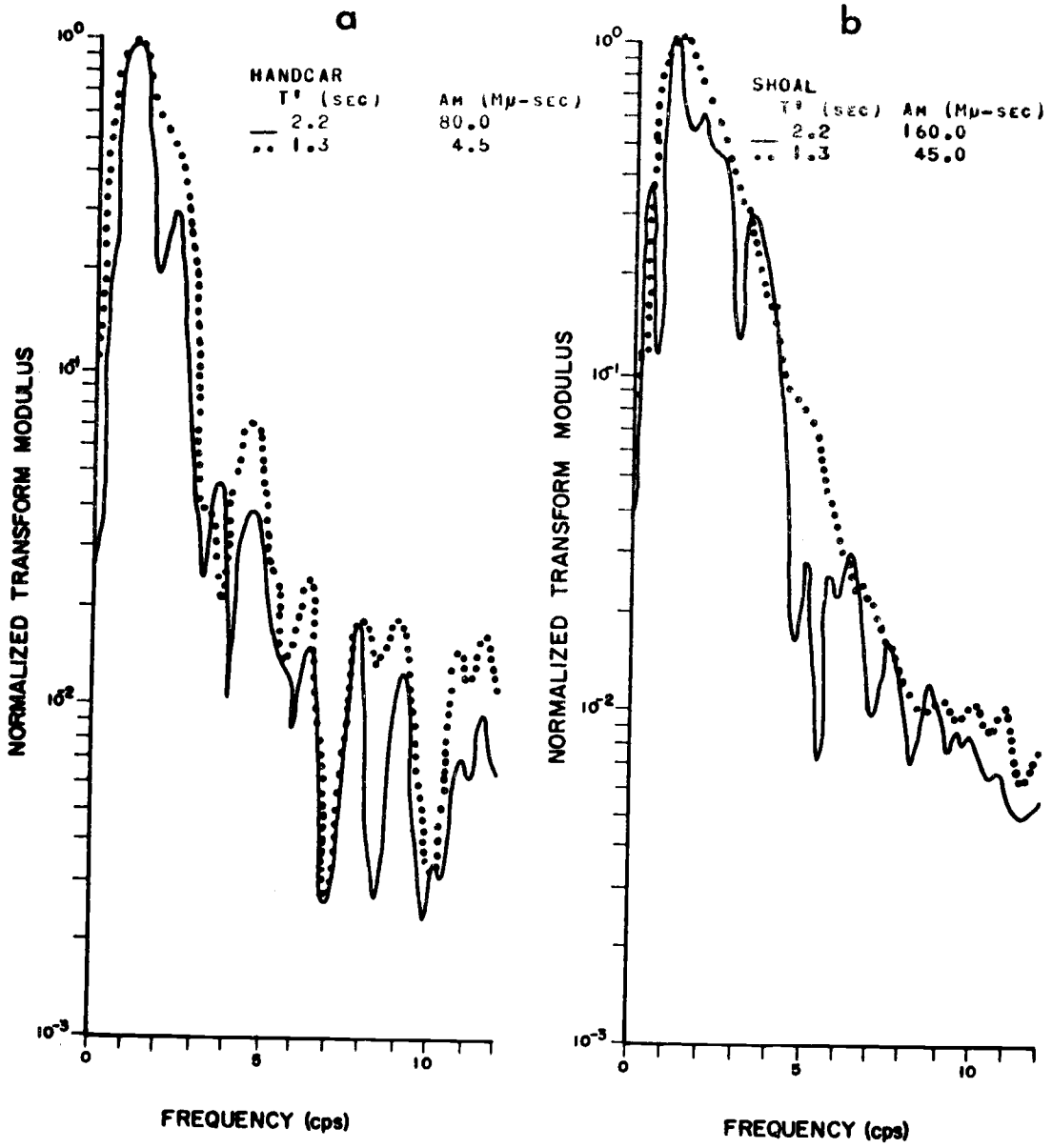

Figure 15. The spectral amplitudes of the (a) Handcar and (b) Shoal output signals recorded at station UBSO.
T' = time duration of the output signals.
Am = the maximum amplitudes of each spectrum.

at 4.0 seconds, but the spectrum was similar to that of the 2.2 seconds signal and for that reason is not shown. The peak amplitudes of the spectra were normalized for comparison. The actual peak amplitude (Am) of each spectrum is given in the figure. Each spectrum peaked at 1.2 cps and decreased very rapidly to ten percent of the peak amplitude at three cps and to one percent of the peak amplitude at six cps. Although the passband of reliable frequencies ($0.2 \leqslant f \leqslant 3$ cps) was not changed by increasing the duration of the signals, the amplitude and character of the output spectra were altered due to the increased frequency resolution and to the large amplitudes after the third half-cycle of the output signal. These spectra of the Handcar signal are similar to the spectra calculated for all of the signals recorded from the explosions in the Nevada Test Site.

The output signal from the Shoal explosion was truncated at 1.1 and 2.2 seconds (see Figure 6c), and the spectral amplitudes for the truncated signals are shown in Figure 15b. The spectrum of the 2.2 seconds duration signal was complicated due to the modulating effects of a large amplitude secondary arrival at about 1.1 seconds reduced time. The peak spectral amplitude for the signal

truncated at 2.2 seconds was three times the amplitude of the signal truncated at 1.1 seconds (see Figure 15b). The Shoal spectra were broader than those for the Handcar signals due to the differences in the propagation paths from the two explosions.

Even though the amplitudes of the output signals of the Handcar explosion were anomalous, as discussed earlier, the Handcar explosion was selected to calibrate station UBSO because it was the only source recorded at UBSO from NTS for which the input signal was known. The source spectra and source functions derived using output signals truncated at 1.3 and 2.2 seconds for the Pile Driver explosion are shown in Figure 16a (Handcar calibration). The maximum amplitudes of the derived source spectra were located at frequencies between three and eight cps, and were outside of the passband of reliable frequencies for the output spectra ($0.2 \leqslant f \leqslant 3$ cps). Within the passband of reliable frequencies, the amplitudes of the derived source spectra peaked at 1.8 cps. The source functions derived for Pile Driver, using output signals of 2.2 and 1.3 seconds duration and using the reliable frequencies, are shown in Figure 16a. Only the reliable frequencies were used to derive the source

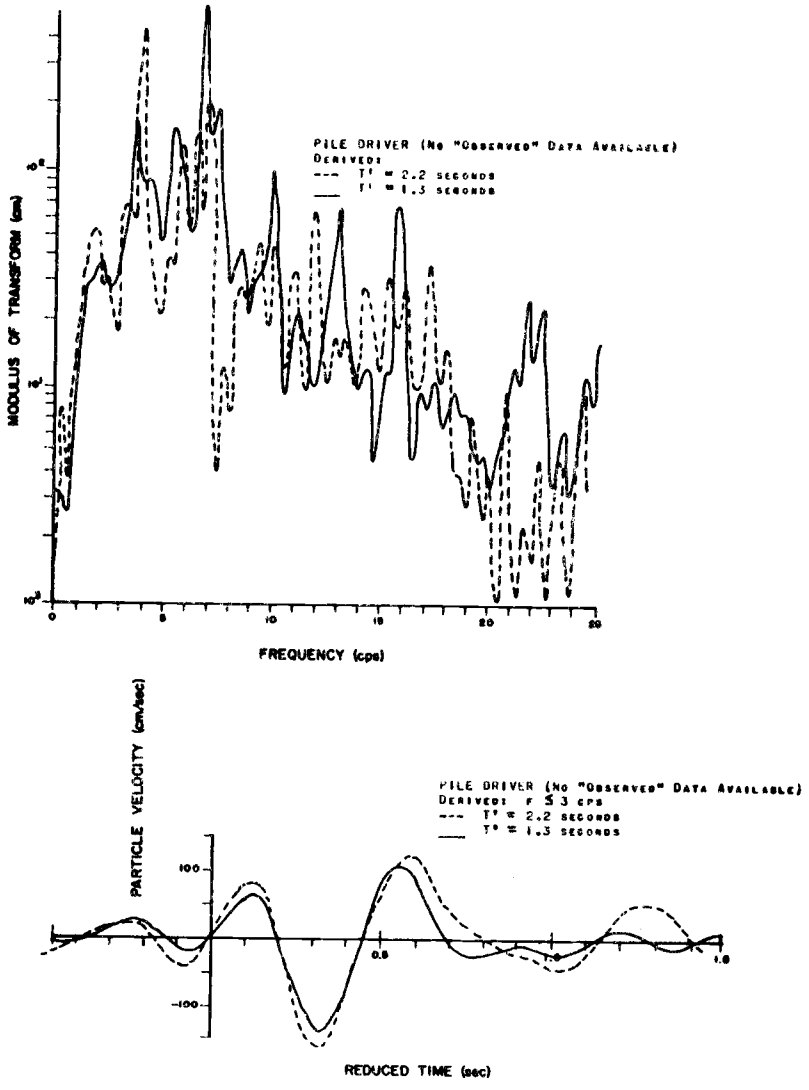

Figure 16a. Comparison of the "observed" and derived source spectra and source signals for the Pile Driver (no "observed" data available) explosion. Station UBSO - Handcar calibration.

T' = time duration of the output signals used.

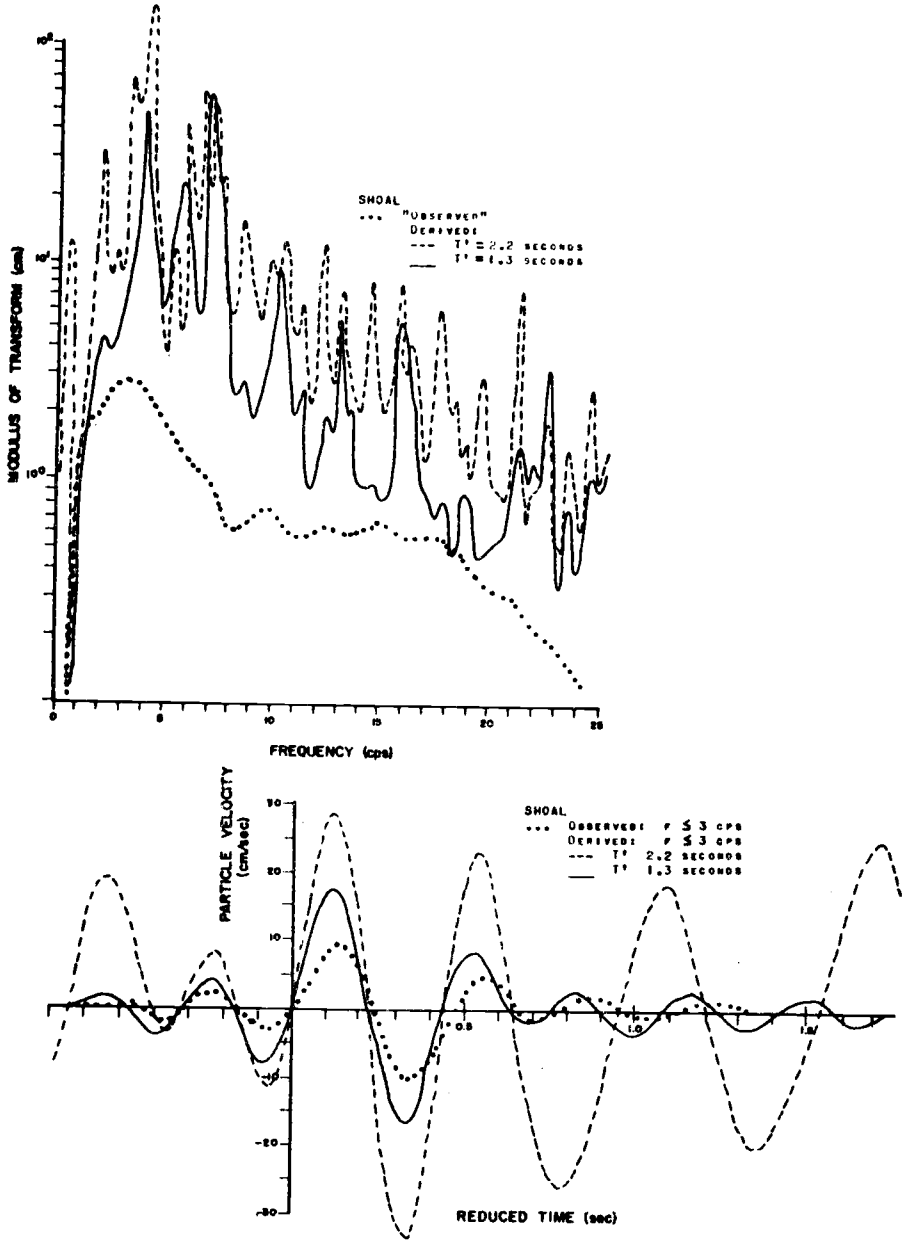

Figure 16b. Comparison of the "observed" and derived source spectra and source signals for the Shoal explosion. Station UBSO - Handcar calibration.

T' = time duration of the output signals used.

functions because the spikes at four and six cps in the derived spectra were dominant, and, therefore, the source functions derived using all frequencies were essentially sine waves osciallating over the complete five second fundamental period.

The source spectra derived for the Shoal explosion using the output signal truncated at 1.3 and 2.2 seconds are compared to the "observed" source spectrum in Figure 16b (Handcar calibration). The source spectrum derived using the 2.2 seconds duration output signal was very oscillatory even within the passband of reliable frequencies, and the spectral amplitudes were greater than those of the "observed" source spectrum. The source spectrum derived using the output signal of 1.3 seconds duration was less oscillatory within the passband of reliable frequencies but was dominated by large amplitude spikes for frequencies greater than three cps.

The source functions derived for Shoal using only the frequencies less than three cps in the derived source spectra are compared to the observed Shoal source function for the same frequencies in Figure 16b. As before, the precursor in the observed source function was due to the ideal low-pass filter that was used in this analysis.

The source function derived using the reliable frequencies of the output signal truncated at 1.3 seconds was similar in shape to the observed source signal ($f \leqslant 3$ cps), but the source signal derived using the output signal truncated at 2.2 seconds was not. This was due to the effects of the spikes in the spectra for frequencies less than three cps which resulted from the large amplitude secondary arrivals in the output signal from Shoal. Both of the derived source functions were greater in amplitude than the observed source function due to the small amplitude of the Handcar signal recorded at station UBSO.

The source energies of the Bilby, Pile Driver, and Shoal source signals, which were derived (Handcar calibration) are shown in Table IV. The frequencies and duration of the output signals are shown in the table also.

The energies derived for the Bilby and Shoal sources were quite dependent upon the duration of the output signals. This was due to secondary arrivals of large amplitudes after 1.3 seconds in the Bilby and Shoal output signals. Possibly due to the anomalously small signal that was propagated to large epicentral distances, the arrival at 1.3 seconds was not evident in

TABLE IV: Comparison of seismic energies of "observed" and derived sources (UBSO - Handcar calibration).

Explosion	Frequencies used (cps)	"Observed" source energy ($\times 10^{18}$ ergs)	Source energy derived using output signals of duration: 4.0 sec. ($\times 10^{18}$ ergs)	2.2 sec. ($\times 10^{18}$ ergs)	1.3 sec. ($\times 10^{18}$ ergs)
Bilby	$f \leqslant 25$		17000.	1500.	3100.
	$f \leqslant 3$	42. *	150.	170.	38.
Pile Driver	$f \leqslant 25$		13000.	5600.	10000.
	$f \leqslant 3$	**	120.	160.	160.
Shoal	$f \leqslant 25$	4.6		1900.	190.
	$f \leqslant 3$	1.9		32.	3.4

* Estimated from close-in surface measurements (Sarmah, 1966).
** No information available.

the Handcar output signal (see Figure 6b). Consequently it was not incorporated into the calibration. The modulating effect of the secondary arrivals caused large amplitude spikes in the source spectra derived using the output signals truncated at 2.2 seconds. However, when shorter duration output signals were used, the spikes in the derived spectra were not present, due to the removal of the secondary arrivals and due to the reduced frequency resolution resulting from shortening the pulse. Since the Handcar and Pile Driver output signals at UBSO were similar in character (see Figure 6b), the source energy computed for the Pile Driver explosion was less dependent upon the duration of the output signal when only frequencies less than three cps were considered. It should be added, that the character of the signal from central Nevada (Shoal) was considerably different from those from the Nevada Test Site (Bilby and Pile Driver) due to the differences in the propagation paths.

The differences in the output signals after 1.3 seconds, resulting from secondary arrivals, caused the energies derived using the 2.2 seconds duration signals to be questionable. Therefore, the most reliable estimates of the source energies were those derived using

frequencies less than three cps and using output signals of 1.3 seconds duration (underlined in Table IV).

Teleseismic distance. - The seismic signals recorded at stations MBC and NP-NT were shown in Figure 6c and 6d, and the synthesized output signals, applicable for Handcar and Haymaker at MBC and Shoal at NP-NT, were shown in Figure 10. The synthesized pulses were approximately 2.5 seconds duration for all of the sources.

Although the responses of the recording systems at stations MBC and NP-NT differed (see Figure 5), the waveforms of the Bilby, Shoal, and Pile Driver signals recorded at the two stations were quite similar, and maximum amplitudes were within 20 percent of each other. The Shoal signals at MBC and NP-NT are compared in Figure 17a, and the Fourier spectra of the signals are compared in Figure 17b. (The arrow indicates the duration of the signals used in the frequency analysis). Both spectra peaked at one cps and decreased very rapidly (20 decibels per octave) to ten percent of the peak amplitude by 2 cps. At frequencies above three cps, where the amplitudes were less than five percent of the peak amplitudes, the spectra differed, both in character and amplitude, due to the different digitizing procedures used and also due to the

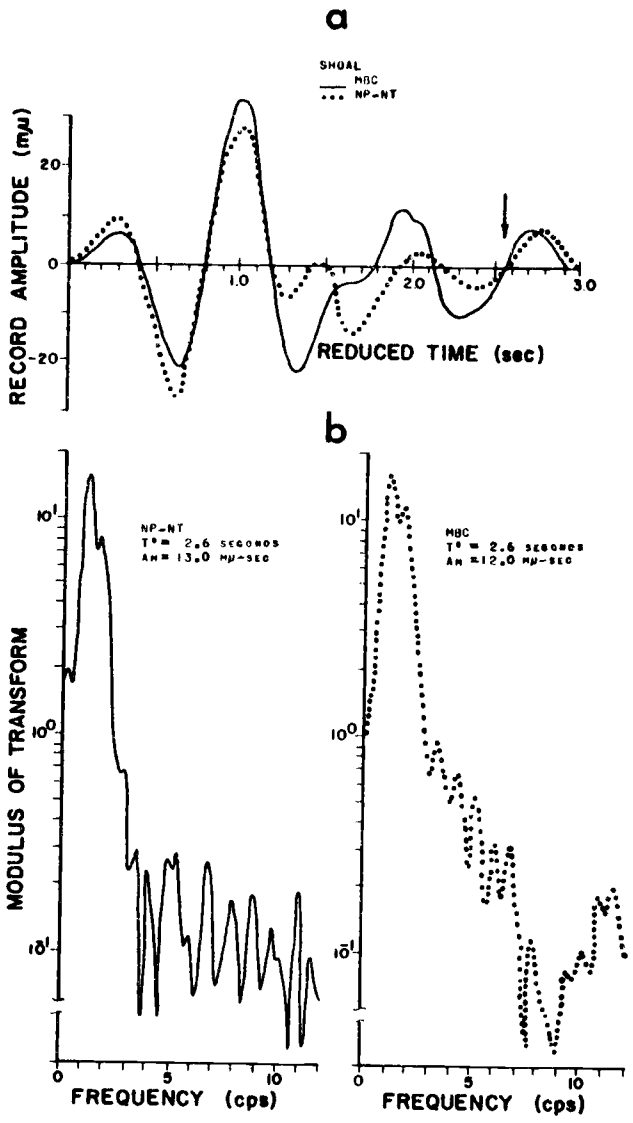

Figure 17. Comparison of the (a) signals and (b) spectral amplitudes of the Shoal output signals at stations MBC and NP-NT.

predominance of noise in the spectra at these frequencies. However, for the passband of reliable frequencies ($0.2 \leqslant f \leqslant 2.0$ cps) it was found that the output signal spectrum at station MBC was similar to that at station NP-NT. In the following analysis, only the results for station MBC are presented.

The spectral amplitudes obtained using 1.2, 2.5, and 5.0 seconds of the observed signals from the Haymaker and Handcar explosions are shown in Figure 18. The folding frequency of the data was 25 cps, but the amplitudes for frequencies above 12 cps are not shown in Figure 18 because they were less than one percent of the peak amplitudes of the spectra. The peak amplitudes of the spectra were normalized for comparison of the shapes, but the absolute values of the peaks (Am) are given in the figure. As the duration of the output signals was increased, the peaks of the spectra became more pronounced. This was due to the increased frequency resolution and also due to the effects of the secondary arrivals, occurring between 1.0 and 1.5 seconds, which were included in the longer duration signals. Since the passband of reliable frequencies was so narrow ($0.2 \leqslant f \leqslant 2.0$ cps), the modulating effect of the secondary arrivals was mainly to increase the peak

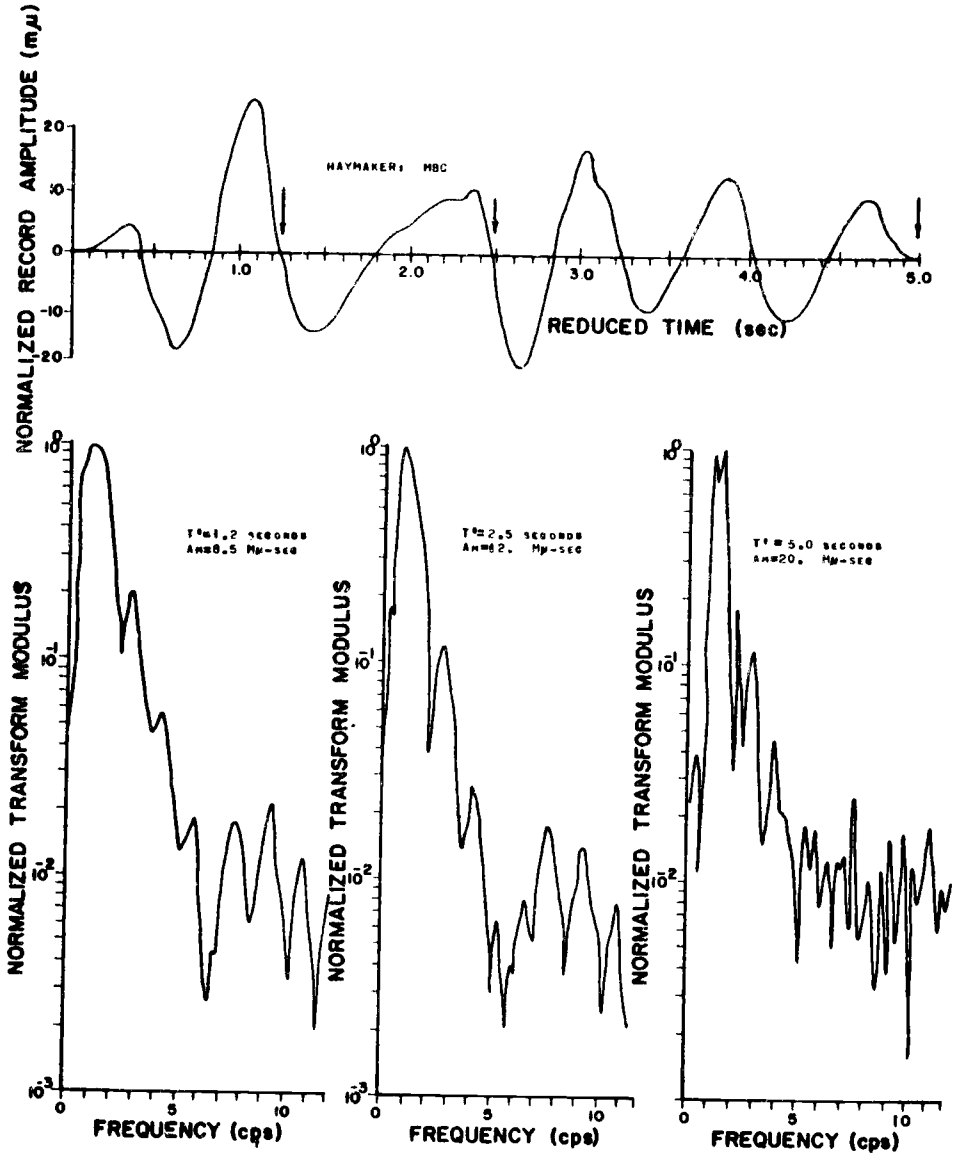

Figure 18a. Station MBC - the output signals and spectral amplitudes of the Haymaker explosion.

T' = time duration of the output signals used.

Am = the maximum amplitude of each spectrum.

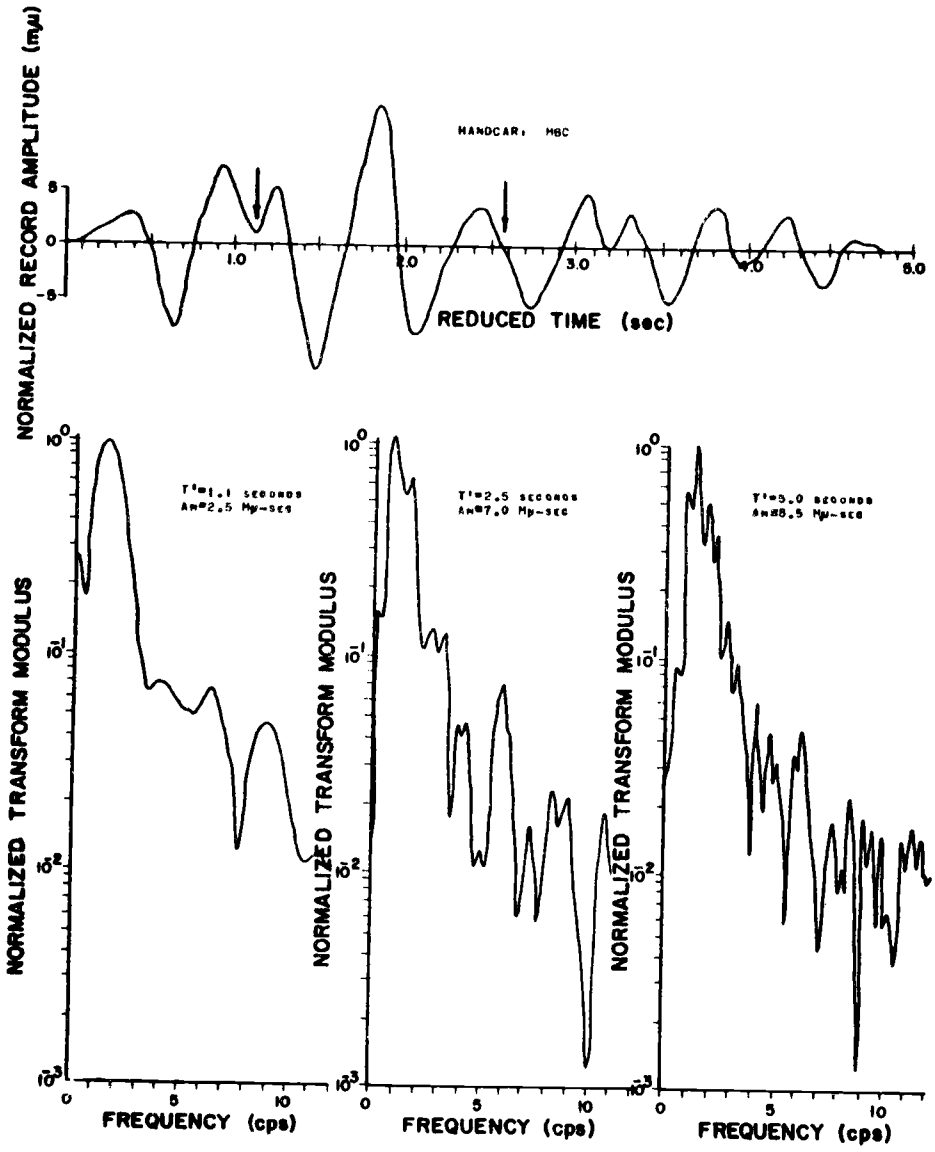

Figure 18b. Station MBC - the output signals and spectral amplitudes of the Handcar explosion.

T' = time duration of the output signals used.

Am = the maximum amplitude of each spectrum.

amplitudes of the spectra (see the values of Am in Figure 18). Therefore, while the passband of reliable frequencies was not significantly changed by using signals of different time duration, the amplitudes of the spectra were affected.

Since the synthesized signals for teleseismic distances were in some cases more similar to the observed signals when a surface reflection was included in the synthesis (see Figure 10b), a reflection from the free surface at the source may be present in the observed output signals. However, the effect of the surface relfection on the character of the synthesized output signals was subtle due to the very narrow passband of dominant frequencies. No conclusions as to the presence of the surface reflections in the observed output signals could be drawn from the character of the output spectra.

The Shoal explosion (central Nevada) was used to calibrate station MBC for the explosions in the Nevada Test Site. Although the epicentral distance from the Shoal explosion to station MBC was approximately 300 kilometers less than that from the other explosions (see Table II), the difference in epicentral distance was small compared to the total propagation path. The azimuth from

the sources to the station were nearly the same (see Figure 3).

The source spectrum derived for the Haymaker explosion using output signals truncated at 2.5 and 5.0 seconds are compared to the "observed" source spectrum for the Haymaker explosion in Figure 19a. The source spectrum derived using output signals truncated at 1.2 seconds did not differ greatly from that derived using output signals truncated at 2.5 seconds, and for that reason the former is not shown in Figure 19a. The spectrum derived using the 5.0 seconds duration output signals was very complex, even within the passband of reliable frequencies. It was dominated by large amplitude spikes centered about three cps. The source spectrum derived using output signals truncated at 2.5 seconds was similar in shape but less in amplitude than that of the "observed" spectrum for the reliable frequencies ($f \leqslant 2.0$ cps). The large amplitudes in the derived spectra at frequencies $2.2 \leqslant f \leqslant 4$ cps were due to the presence of secondary maxima in the Haymaker output spectra which were not present in the calibration (Shoal) output spectra (see Figures 17b and 18b).

The source functions derived for Haymaker ($f \leqslant 2$ cps) from the above spectra using the inverse Fourier transform

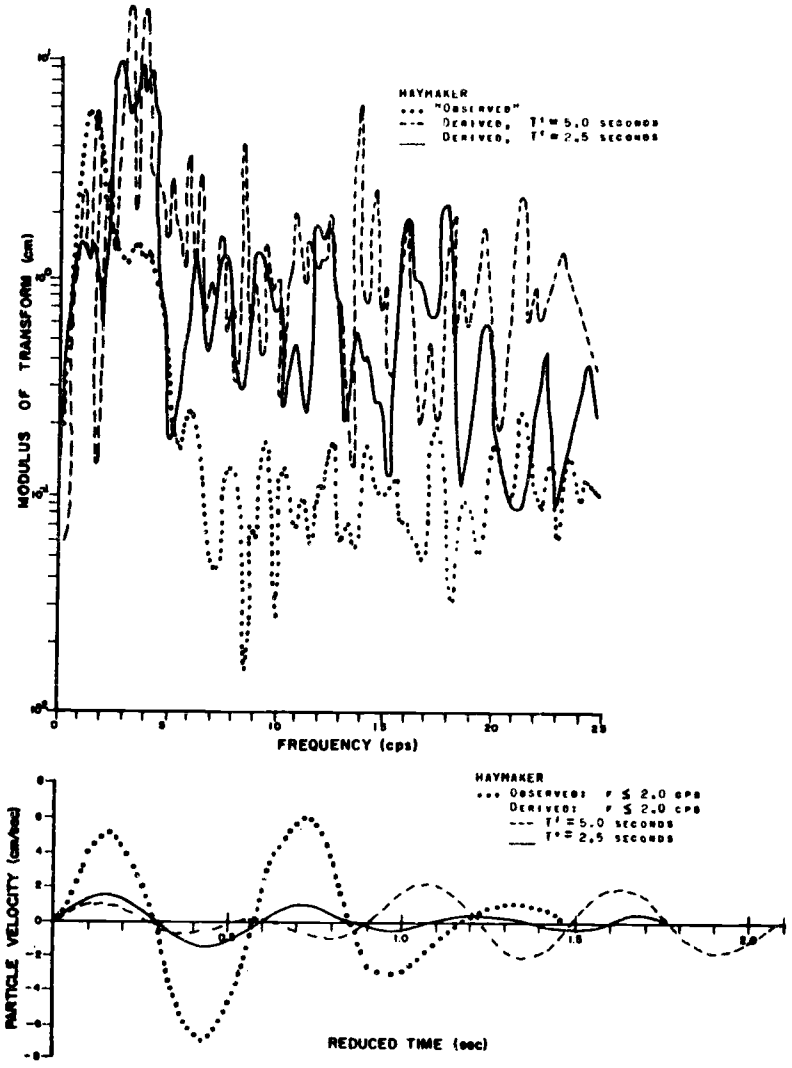

Figure 19a. Comparison of the "observed" and derived source spectra and source signals for the Haymaker explosion. Station MBC - Shoal calibration.

T' = time duration of the output signals used.

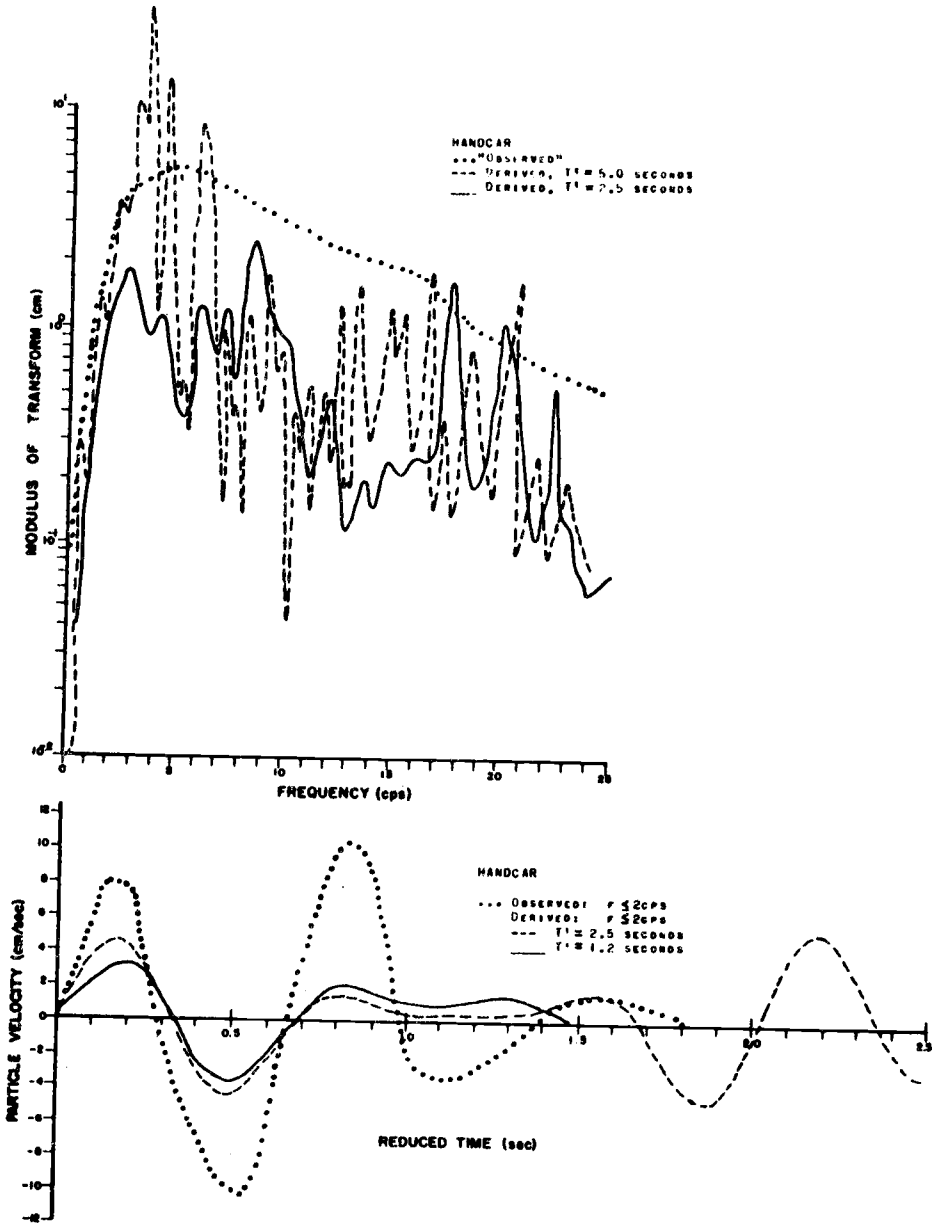

Figure 19b. Comparison of the "observed" and derived source spectra and source signals for the Handcar explosion. Station MBC - Shoal calibration.
T' = time duration of the output signals used.

are compared in Figure 19a to the observed source function. The source function obtained using the 2.5 seconds duration output signals was similar in shape to the "observed" source function, but the amplitudes were only approximately 25 percent of the observed amplitudes. The source function for the Haymaker explosion, which was derived using the 5.0 seconds duration output signals, was more complicated that the observed source signal and appeared as a multiple source signal due to the spikes in the derived spectrum within the passband of frequencies used ($f \leqslant 2$ cps).

The source spectra for the Handcar explosion, which were derived using output signals truncated at 1.2 and 2.5 seconds, are shown in Figure 19b. The modulating effects of the secondary arrival at 1.3 seconds reduced time in the Handcar output can be seen in the figure also. Within the passband of reliable frequencies ($f \leqslant 2$ cps), the spectrum derived using the longer duration output signals (2.5 seconds) contained spikes which were not present in the spectrum derived using the shorter duration signal; the spikes were not present in the "observed" source spectrum either. Outside the passband of reliable frequencies, the two derived spectra differed in amplitude

from the "observed" spectrum by an order of magnitude. The source spectrum derived using the output signals truncated at five seconds was similar to that derived using the output signals of 2.5 seconds time duration.

The source functions derived for the Handcar explosion ($f \leqslant 2$ cps) using the inverse Fourier transform are compared to the observed source signal in Figure 19b. The waveform of the source function derived using the output signal of 2.5 seconds time duration was complex and was not similar to the observed source signal. This is due to the effects of the secondary arrival at 1.3 seconds reduced time. The waveform of the source function derived using the output signals of 1.2 seconds duration was somewhat similar to the observed source function, but the derived amplitudes were only approximately 30 percent of the observed source amplitudes.

The seismic energies of the derived source functions for the Haymaker, Bilby, Handcar, and Pile Driver explosions were calculated from the derived source spectra and are compared to the energies of the observed source signals in Table V.

The seismic energies computed using all frequencies ($f \leqslant 25$ cps) were very dependent upon the time duration

TABLE V: Comparison of seismic energies of "observed" and derived sources (MBC - Shoal calibration).

Explosion	Frequencies used (cps)	"Observed" source energy ($\times 10^{18}$ ergs)	Source energy derived using signals of duration: 5.0 sec. ($\times 10^{18}$ ergs)	2.5 sec. ($\times 10^{18}$ ergs)	1.2 sec. ($\times 10^{18}$ ergs)
Haymaker	$f \leqslant 25$	0.89	73.	17.	8.2
	$f \leqslant 2$	0.75	1.4	0.43	0.43
Bilby	$f \leqslant 25$			28000.	770.
	$f \leqslant 2$	42. *		32.	37.
Handcar	$f \leqslant 25$	8.0	56.	39.	0.84
	$f \leqslant 2$	0.51	0.72	0.21	0.08
Pile Driver	$f \leqslant 25$	**	11000.	4200.	210.
	$f \leqslant 2$		66.	20.	12.

* Estimated from close-in surface measurements.
** No information available.

of the output signals. This resulted from the predominance of noise at the high frequencies in the output spectra. When only frequencies less than two cps were used the source energy varied by a factor or three, approximately, for signals of different time durations. For the Handcar explosion, the variation was an order of magnitude. This large variation resulted from the secondary arrival at 1.2 seconds in the Handcar output signal. Therefore, although the duration of the synthesized signals for station MBC indicated that the primary waves were at least 2.0 seconds duration (see Figure 10), the character of the output signals of greater duration than 1.2 seconds were contaminated by secondary arrivals. The calibration did not adequately include the effects of the later arrivals. Therefore, the most reliable derived source energies were those obtained using frequencies less than two cps and output signals of 1.2 seconds duration. These values are underlined in Table V, and are 60, 90, and 16 percent of the "observed" source energies for the Haymaker, Bilby, and Handcar explosions, respectively.

SUMMARY AND CONCLUSIONS

The lumped earth-receiver system for a given source and recording station includes the effects of: (1) the source environment, (2) the propagation path, and (3) the receiver system at the station. The operator for this system was called the lumped calibration operator. A method was presented to determine the lumped calibration operator from a source signal observed near the elastic-inelastic boundary of an underground explosion and from an output signal observed at a distant recording station. In principle, the lumped calibration operator could be used to determine information about other sources from their output signals at the calibrated stations. This method of calibration was applied to the primary waves from six underground nuclear explosions recorded at stations located at near-regional, regional, and teleseismic distances. The important implications and conclusions resulting from this research are discussed in this chapter in three sections. In the first section, the constraints that limit the capabilities of the method of calibration are summarized. In the second section, the method of calibration is evaluated, and in the final section the conclusions of

of this research are presented.

Summary of constraints

The constraints that limit the capabilities of the calibration method are: (a) the source-propagation path-receiver system (earth-receiver) acts as a band-pass filter which limits the amount of source-related information contained in the output signals; (b) the contamination of the pure primary waves by secondary arrivals limits the time duration of the usable portions of the output signals; and (c) the lumped calibration operators may vary significantly for the different explosions due to differences in the locations of the sources.

Constraint (a): The most obvious constraint on the method of calibration was that the earth-receiver system acted as a narrow band-pass filter. The information contained in the output signals that could be reliably related to the sources was confined to the frequency passbands $0.2 \leqslant f \leqslant 4.0$ cps, $0.2 \leqslant f \leqslant 3.0$ cps, and $0.2 \leqslant f \leqslant 2.0$ cps at the near-regional, regional, and teleseismic stations, respectively. The low-frequency cutoff of these passbands was due mainly to the insensitivity of the short-period recording instruments to the low frequencies.

The high-frequency cutoff was due to the attenuation of the earth. For frequencies outside of these passbands the spectral amplitudes were attenuated to such low levels that noise caused by the digital techniques (mainly limitations on the accuracy of the digitizing) was dominant.

Constraint (b): The seismograms obtained at the distant stations consisted of many arrivals which propagated to the stations by different paths. The first arrivals (primary waves) were used as the output signals because there was the least uncertainty about the onset of these arrivals. However, some ambiguity in the definition of the output signals was encountered because other pulses interfered with the initial arrival. The observed source signals were used to synthesize pulses at the distant stations to aid in determining the time duration of the primary waves. Portions of the observed first arrivals which were shorter than, equal to, and longer than the durations of the synthesized pulses were used in the analysis to test the effects of pulse duration on the derived source signals. The derived source characteristics varied for different time durations of the first arrivals due to the effects of interfering arrivals and noise.

Constraint (c): Differences in the locations of explosions can cause variations in the lumped calibration operator for a recording station. When the explosions are near one another, compared to the epicentral distance, the major portions of the propagation paths are the same. In this case, variations in the calibration operator are most likely due to differences in the source environments (i.e. local geology, media, and/or depths). However, when the differences in the locations of the explosions are large, compared to the total propagation path, then major portions of the wave paths differ. In this case, variations in the calibration operator are due to the combined effects of differences in source environments and the propagation paths. Hence, differences in the locations of the sources constitute another constraint of the method of calibration.

Evaluation of the method of calibration

Information about the source functions (spectra, waveforms, and energy content) could be derived only within the passbands of reliable frequencies defined by the spectra of the output signals. Outside of these passbands, noise (which, by definition, was not source-

related) dominated the information contained in the output signals. Due to this limitation (on the high frequencies, mainly), all of the derived source functions were similar in character, as were the observed source functions when filtered to these passbands. Therefore, the method of calibration cannot be used to derive impulsive source functions when the frequency content of the output signals is so limited. The spectra and the energies of the derived source functions were also confined to the above passbands.

The passbands of reliable frequencies may be broadened if output signals from stations located closer to the sources are used. However, the effects of interfering secondary arrivals may severely limit the usable time duration of the output signals at these stations. If the lumped calibration operators for the calibration and unknown sources are the same, then secondary arrivals will not affect the results of the method of calibration (see equation 42 in Appendix II). Secondary arrivals modulate the spectra of the primary waves, and the characteristics of the modulation are governed by their amplitudes, waveforms, and delay times (see equations 40 and 41, and Figure 20 in Appendix II). As the time duration of output

signals is increased, secondary arrivals are included which may not be adequately incorporated into the lumped calibration operator. This effect may result from any secondary arrival, regardless of its derivation (surface reflection or pulse from a different propagation path). This effect was most evident in the case of the output signals at the regional station (UBSO). The output signal for the Shoal explosion was significantly different in character from the signals from explosions in the Nevada Test Site (see Figures 6b and 15). These differences were due mainly to the significant differences in the propagation paths to the station (see Figure 3).

There was uncertainty as to whether or not surface reflections contaminated the primary waves. If they were present in the output signals, the delay times would be small for the data used in this research, and the modulation of the output spectra would have been broad (see Figure 20 in Appendix II). Since the passbands of reliable frequencies were narrow at the regional and teleseismic stations, the effects of the reflections on the primary waveforms would have been subtle, and their effects on the method of calibration would not have been great (see Figures 21 and 22 in Appendix II). At the

near-regional station, where the passbands of reliable frequencies were broader, the effects of other secondary arrivals and noise precluded the determination of their presence. However, it was noted that the pulses synthesized at the near-regional distance (station MN-NV) were most similar to the observed signals when no reflections were included in the synthesis (see Figure 10). More research is needed to determine if these reflections are present in the output signals, because if they are, their effects can be very important at small epicentral distances.

The most reliable source information was derived when only three half-cycles of the output signals were used in the method of calibration at all of the stations. The seismic energies derived using this duration of output signals and using frequencies within the passbands of reliable frequencies are compared to the seismic energies of the observed source functions in Table VI.

The deviations of the derived source energies from the "observed" source energies were due mainly to differences in the near-source propagation losses caused by variations in the local geology and in the media surrounding the different explosions. The Handcar explosion was

TABLE VI: Comparison of the "observed" and the most reliable derived source energies.

Explosions	Medium	Energy $x10^{18}$ ergs $0.2 \leqslant f \leqslant 4$ cps		Energy $x10^{18}$ ergs $0.2 \leqslant f \leqslant 3$ cps		Energy $x10^{18}$ ergs $0.2 \leqslant f \leqslant 2$ cps	
		"Observed"	Derived MN-NV	"Observed"	Derived UBSO	"Observed"	Derived MBC
Hardhat	granite	Calibration event		not recorded		not recorded	
Shoal	granite	Data not used		1.9	3.4	Calibration event	
Pile Driver	granite	**	42.	**	160.	**	12.
Handcar	dolomite	3.2	0.22	Calibration event		0.51	0.08
Bilby	tuff	42. *	37.	42. *	38.	42. *	37.
Haymaker	alluvium	0.82	0.58	not recorded		0.75	0.43

* Estimated from close-in surface measurements, (Sarmah, 1966).
** No information available.

the only source used in this research for which the effects of the near-source losses on the derived source energies were extreme (see Table VI). There have been several explanations suggested for the anomalously low amplitudes of the output signals from the Handcar explosion (Springer, 1966). Regardless of the cause of the large energy loss associated with the signals from this explosion, it is obvious that anomalous signals will severely limit the effectiveness of any calibration method.

When the environments of the sources are known, then the results of the method of calibration can be improved by using calibration sources for which the source environments (local geology, media, and depths) are as similar as possible to those of the unknown sources. However, the source environments of explosions cannot, at this time, be determined from output signals (primary waves). Therefore, any attempt to apply the method of calibration to output signals from unknown sources (with no information about the source environments) would have to be done on the basis of an average source-propagation path - receiver system. The average calibration operator would have to be determined using data from many different

explosions located in varying source environments. It was not possible to do this for this research.

The relation between the derived source energies given in Table VI and the total seismic energy (energy contained in all frequencies) at the sources is complex, as implied by the variations in the spectral distribution of the seismic energy of the observed source functions (see Figure 8d). These variations were due to the coupling characteristics which are dependent upon the medium and/or depth of the explosions. The charge size of explosions may also affect the spectral distribution of the seismic energy at the sources, but no observed data were available to determine the importance of this effect. However, Berg and Papageorge (1964) showed that, for a theoretical source in an infinite homogeneous medium, the relative amount of energy concentrated in the low frequencies increased with increasing charge size. If this is the case for underground explosions, then as the size of the explosions in a given medium increased, the relative amount of seismic energy concentrated in the high frequencies would decrease. Subsurface data near explosions of differing sizes in the same medium (and same depth) are needed to determine the effects of the charge

size on the spectral distribution of the seismic energy generated by explosions. This information would be necessary to relate the source energy derived in limited frequency bands to the seismic energy in all frequencies at the sources (see Figure 8d).

The conclusions about the capabilities of the method of calibration pertain only to the initial P waves generated by explosions in Nevada and recorded by stations located in the northern direction from Nevada. It seems reasonable to expect that these conclusions would not be greately different if the explosions and/or recording stations were located in other areas, but more research is needed in order to determine the extent to which the capabilities of the method of calibration may vary.

Conclusions

1. A seismograph station can be calibrated by an explosion at a given site. The output signals recorded at that station can be used to derive information about other sources at the same site. For the data used in this research, the most significant source information derived from output signals was the source energy that was related to the distant signals. The criteria for

selecting a calibration source are: (1) the source function must be known; (2) the source function should be impulsive in order to calibrate the stations for as many frequencies as possible; and (3) the signal levels at the stations should be large in order to minimize the effects of noise.

2. The source-propagation path-receiver system acts as a band-pass filter which limits the amount of source-related information contained in the output signals. The passbands were limited on the low-frequency end by the insensitivity of the short-period recording instruments to the low frequencies and on the high-frequency end by the attenuation of the earth. The passbands of reliable frequencies were: $0.2 \leqslant f \leqslant 4.0$ cps, $0.2 \leqslant f \leqslant 3.0$ cps, $0.2 \leqslant f \leqslant 2.0$ cps at the near-regional, regional, and teleseismic stations, respectively.

3. Information about the source functions (i.e. waveforms, spectra, and energy content) could be derived only within the above passbands of reliable frequencies. All of the derived source functions were similar in waveform due to the limitations on the

high frequencies that could be utilized. The observed source functions were also similar when filtered to the above passbands. It is implied, therefore, that pulses synthesized for regional and teleseismic distances will be very similar in character regardless of the source functions.

4. The results of the method of calibration differed as the time duration of the output signals was varied due to the effects of interfering secondary arrivals which were not adequately included in the calibrations. The most reliable results were obtained when only three half-cycles of the output signals were used in the analysis. Reflections, from the free surface at the sources, could not be identified in the output signals due to the narrow passbands of reliable frequencies, and due to the effects of other secondary arrivals. If such reflections are present in output signals, their effects can be very significant at near-regional stations, but their effects are not great at teleseismic stations.

5. Differences in the near-source propagation losses caused the most reliable values of the derived source

energies to deviate from the "observed" source energies. For the stations calibrated using explosions in granite, the average values of the most reliable source energies derived for the explosions in tuff, alluvium, and dolomite were 88, 65, and 12 percent of the "observed" source energies, respectively. More research is necessary to determine the specific causes of these large variations in derived source energies.

6. The environment of a calibration source should be as similar as possible to the source environments of the events for which information is to be derived. When the method of calibration is applied to events for which no such information is available, then the calibration operator should be representative of the best average source-propagation path-receiver system.

7. The spectral distribution of the seismic energy generated by the explosions was a function of the media in which the sources were located. Near the elastic-inelastic boundaries, only ten percent of the seismic energy generated by the explosion in alluvium was concentrated in the frequencies greater than two cps,

whereas ninety percent of the seismic energy generated by the explosions in granite and dolomite were concentrated in these frequencies.

8. The effects of secondary arrivals in the observed source waveforms were negligible for the purpose of this research.

9. The recordings of particle velocity obtained at the subsurface stations include a component which is not propagated to large epicentral distances (Berg and Papageorge, 1964). In this research, it was found that the waveforms of the radiation field source functions, which resulted from the removal of the above component, were not significantly different from the recorded particle velocity waveforms. However, the amplitudes of the low frequencies ($f \leqslant$ one cps) contained in the radiation field source functions were significantly less than those contained in the "total" pulse (recorded waveform).

10. The first cycle of the pulses synthesized for the near-regional station were similar to the observed recordings when no surface reflections were included.

Secondary arrivals precluded the comparison of the synthesized and observed signals after the first cycle. For the regional station, the synthesized and observed signals were not sufficiently similar to determine whether or not surface reflections improved the comparison. For the teleseismic stations, the comparison between the synthesized and observed signals was somewhat improved when a surface reflection was included. No definite conclusions could be made about the occurrence of surface reflections.

BIBLIOGRAPHY

Ben-Menahem, A., S. W. Smith and T. L. Teng. 1965. A procedure for source studies from spectrums of long-period seismic body waves. Bulletin of the Seismological Society of America 55: 203-235.

Berg, J. W., Jr. and L. T. Long. 1966. Characteristics of refracted arrivals of seismic waves. Journal of Geophysical Research 71: 2583-2590.

Berg, J. W., Jr. and G. E. Papageorge. 1964. Elastic displacement of primary waves from explosive sources. Bulletin of the Seismological Society of America 54: 947-960.

Berg, J. W., Jr., L. D. Trembly and P. R. Laun. 1964. Primary ground displacements and seismic energy near the GNOME explosion. Bulletin of the Seismological Society of America 54: 1115-1126.

Bogert, B. 1962. Correction of seismograms for the transfer function of the seismometer. Bulletin of the Seismological Society of America 52:781-792.

Bullen, K. E. 1963. An introduction to the theory of seismology. 3d ed. Cambridge, Cambridge University Press. 381 p.

Carpenter, E. W. 1964. Teleseismic methods for the detection, identification, and location of underground explosions. Ann Arbor, University of Michigan, Institute of Science and Technology. 69 p. (VESIAC State-of-the-Art Report 4410-67-X, Contract SD-78)

Carpenter, E. W. 1966. A quantitative evaluation of teleseismic explosion records. Proceedings of the Royal Society (London), ser A, 290: 396-407.

Carpenter, E. W. 1967. Teleseismic signals calculated for underground, underwater, and atmospheric explosions. Geophysics 32: 17-32.

Carpenter, E. W., R. A. Savill and J. K. Wright. 1962. The dependence of seismic signal amplitudes on the size of underground explosions. Geophysical Journal of the Royal Astronomical Society 6: 426-440.

Clewell, D. H. and R. F. Simon. 1950. Seismic wave propagation. Geophysics 15: 50-60.

Fuchs, Karl. 1966. The transfer function for P-waves for a system consisting of a point source in a layered medium. Bulletin of the Seismological Society of America 56: 75-108.

Futterman, W. I. 1962. Dispersive body waves. Journal of Geophysical Research 67: 5279-5291.

Geotechnical Corporation. 1963. Test report, LRSM seismograph calibration study. Garland, Tex. 47 numb. leaves. (Technical Report no. 63-55)

Griggs, D. T. and F. Press. 1961. Probing the earth with nuclear weapons. Journal of Geophysical Research 66: 237-258.

Gutenberg, B. 1944. Energy ratio of reflected and refracted seismic waves. Bulletin of the Seismological Society of America 34: 85-102.

Haskell, N. A. 1962. Crustal reflection of plane P and SV waves. Journal of Geophysical Research 67: 4751-4767.

Herbst, R. F., G. C. Werth and D. L. Springer. 1961. Use of large cavities to reduce seismic waves from underground explosions. Journal of Geophysical Research 66: 959-978.

Howell, B. F., Jr. and D. Budenstein. 1955. Energy distribution in explosion-generated seismic pulses. Geophysics 20: 33-52.

Huang, Y. T. 1966. Spectral analysis of digitized seismic data. Bulletin of the Seismological Society of America 56: 425-440.

Johnson, G. W., G. H. Higgins and C. E. Violet. 1959. Underground nuclear detonations. Journal of Geophysical Research 64: 1457-1470.

Johnson, M. S. and D. E. Hibbard. 1957. Geology of the Atomic Energy Commission Nevada proving grounds area, Nevada. U. S. Geological Survey, Bulletin 1021: 333-384.

Kisslinger, Carl. 1963. The generation of the primary seismic signal by a contained explosion. Ann Arbor, University of Michigan, Institute of Science and Technology. 85 p. (VESIAC. State-of-the-Art Report 4410-48-X, Contract SD-78)

Kisslinger, Carl. 1965. Progress in understanding the generation of seismic waves by contained explosions. Ann Arbor, University of Michigan, Institute of Science and Technology. 23 p. (VESIAC Report 4410-104-X, Contract SD-78)

Latter, A. L., R. E. LeLevier, E. A. Martinelli and W. G. McMillan. 1959. A method of concealing underground nuclear explosions. Santa Monica, Calif. 13 p. (Rand Corporation Report R-348)

Latter, A. L., E. A. Martinelli and E. Teller. 1959. Seismic scaling law for underground explosions. Santa Monica, Calif. 9 p. (Rand Corporation Report P-1594) (Also Physics of Fluids 2: 280-282)

Laun, P. R. 1965. Primary seismic wave (P) at 250-350 km compared to measured wave at 0.3 km from GNOME nuclear explosion. Master's thesis. Corvallis, Oregon State University. 55 numb. leaves.

Nevada. Bureau of Mines. 1962. Geological, geophysical and hydrological investigations of the Sand Springs, Fairview Valley and Fourmile Flat, Churchill County, Nevada for SHOAL event, Project SHADE, VELA UNIFORM program, Atomic Energy Commission. Reno, University of Nevada, Desert Research Institute, Mining Analytical Laboratory. 127 p.

Papoulis, A. 1962. The Fourier integral and its applications. New York, McGraw-Hill. 318 p.

Richter, C. F. 1958. Elementary seismology. San Francisco, Freeman. 768 p.

Sandia Corporation. 1963. Close-in phenomenon of buried explosions. Final report. Albuquerque, N. M. 161 p. (Report SC-4907 (RR))

Sandia Corporation. 1965. Four papers concerning recent work on ground motion measurements. Albuquerque, N. M. 74 p. (Report SC-R-65-904)

Sarmah, S. K. 1966. Attenuation of compressional waves in the earth's mantle. Ph.D. thesis. Corvallis, Oregon State University. 80 numb. leaves.

Smith, S. W. 1965. Generation of seismic waves by underground explosions and the collapse of cavities. Journal of Geophysical Research 68: 1477-1483.

Springer, D. L. 1966. P-wave coupling of underground nuclear explosions. Bulletin of the Seismological Society of America 56: 861-876.

Stephens, D. R. 1964. The hydrostatic compaction of eight rocks. Journal of Geophysical Research 69: 2967-2978.

Sundaram, Seshu and N. Balabanian. 1964. Linear network analysis. 3d. ed. New York, Wiley. 571 p.

Swift, L. M. 1962. Measurement of close-in earth motion: Preliminary report, HARDHAT event, VUP-2101. 63 p. (Stanford Research Institute)

Teng, Ta-Liang and A. Ben-Menahem. 1965. Mechanisms of deep earthquakes from spectrums of isolated body-wave signals. 1. The Banda sea earthquake of March 21, 1964. Journal of Geophysical Research 70: 5157-5170.

Toksöz, M. N., A. Ben-Menahem and D. G. Harkrider. 1964. Determination of source parameters, of explosions and earthquakes by amplitude equalization of seismic surface waves. 1. Underground nuclear explosions. Journal of Geophysical Research 69: 4355-4366.

Trembly, L. D. 1965. Primary seismic waves near explosions. Master's thesis. Corvallis, Oregon State University. 58 numb. leaves.

Trembly, L. D. and J. W. Berg, Jr. 1966. Amplitudes and energies of primary waves near the HARDHAT, HAYMAKER and SHOAL nuclear explosions. Bulletin of the Seismological Society of America 56: 643-653.

Wainstein, L. A. and V. D. Zubakov. 1962. Extraction of signal from noise, tr. by Richard A. Silverman. Englewood Cliffs, N. J., Prentice-Hall. 382 p.

Werth, G. C. and R. F. Herbst. 1963. Comparisons of amplitudes of seismic waves from nuclear explosions in four mediums. Journal of Geophysical Research 68: 1463-1476.

Werth, G. C., R. F. Herbst and D. L. Springer. 1962. Amplitudes of seismic arrivals from the M discontinuity. Journal of Geophysical Research 67: 1587-1610.

Wuenschel, P. C. 1965. Dispersive body waves--an experimental study. Geophysics 30: 539-551.

Wylie, C. R., Jr. 1960. Advanced engineering mathematics. 2d ed. New York, McGraw-Hill. 696 p.

APPENDICES

APPENDIX I

The Fourier Integral transform and inverse transform for continuous functions are given in equations (30) and (31), respectively.

$$g(w) = \left|g(w)\right| e^{i\theta(w)} = \int_{-\infty}^{\infty} F(t)\, e^{-iwt} dt \qquad (30)$$

$$F(t) = \frac{1}{2\pi} \int_{-\infty}^{\infty} g(w)\, e^{+iwt}\, dw, \qquad (31)$$

where: t = time;

w = angular frequency (radians per second);

$i = (-1)^{\frac{1}{2}}$;

$\left|g(w)\right|$ = modulus of the spectrum;

$\theta(w)$ = phase of the spectrum; and

$F(t)$ = function of time.

For numerical data, such as is obtained by digitizing seismograms, the transform pair reduce to finite summations (Huang, 1966). The modulus and phase of the numerical Fourier transform used in this research are given in equations (32) and (33).

$$\left|g(f_k)\right| = (X_k^2 + Y_k^2)^{\frac{1}{2}} \tag{32}$$

$$\theta(f_k) = \tan^{-1}\left(\frac{Y_k}{X_k}\right), \tag{33}$$

where: $X_k = \Delta t \sum_{j=1}^{N} F(t_j) \cos\left(\frac{2\pi jk}{N}\right)$ = real part of the transform for the K<u>th</u> frequency;

$Y_k = \Delta t \sum_{j=1}^{N} F(t_j) \sin\left(\frac{2\pi jk}{N}\right)$ = imaginary part of the transform for the K<u>th</u> frequency;

Δt = digitizing interval;

$F(t_j)$ = the j<u>th</u> value of the digitized time function; and

N = number of samples taken from F(t).

The numerical inverse Fourier transform used in this research is given in equation (34).

$$F(t_k) = \Delta f \left|g(f_o)\right| + 2\Delta f \sum_{j=1}^{N/2} \left|g(f_j)\right| \cos\left(\frac{2\pi jk}{N} + \phi(f_j)\right) - \Delta f \left|g(f_{N/2})\right| \tag{34}$$

where: $\Delta f = \frac{1}{N\Delta t}$ = frequency increment;

f_j = j<u>th</u> frequency (cps); and

$F(t_k)$ = value of the time function at time $k\Delta t$ seconds.

The numerical Fourier transform and inverse transform are periodic, because the data were sampled at a finite number of points (Huang, 1966). The frequency at which the Fourier spectrum is duplicated is equal to twice the folding frequency, f_c, where:

$$f_c = \frac{1}{2\Delta t} \quad . \tag{35}$$

The function of time that results from the application of the finite inverse transform (see equation 34) to a finite Fourier spectrum is also periodic with period equal to the fundamental time period $T = \frac{1}{\Delta f}$. The results of using the transform and inverse transform would be aperiodic only if the sampling intervals (Δt and Δf) were zero (i.e. for continuous functions).

APPENDIX II

The primary waves recorded at distant stations may be contaminated by secondary arrivals such as arrivals from other propagation paths and reflections from the free surface at the sources. The effects of secondary arrivals on the applicability of the method of calibration are considered in this appendix.

An observed output signal is the sum of the primary wave and secondary arrivals as shown in equation (36).

Observed output signal		Primary wave		Secondary arrivals	
$s_{out}(\tau)$	=	$f_{out}(\tau)$	+ $\sum_{j=1}^{N}$	$g_j(\tau - \lambda_j)$,	(36)

where: τ = reduced time in seconds;

$s_{out}(\tau)$ = observed output signal;

$f_{out}(\tau)$ = primary wave;

$g_j(\tau - \lambda_j)$ = jth secondary arrival;

λ_j = delay time of the jth secondary arrival;

N = number of secondary arrivals included in $s_{out}(\tau)$.

In the frequency domain, equation (36) is written as

$$S_{out}(w) = F_{out}(w) + \sum_{j=1}^{N} G_j(w)\, e^{-iw\lambda_j}, \qquad (37)$$

where: $S_{out}(w)$ = Fourier transform of $s_{out}(\tau)$;

$F_{out}(w)$ = Fourier transform of $f_{out}(\tau)$; and

$G_j(w)e^{-iw\lambda_j}$ = Fourier transform of the jth secondary arrival.

If each secondary arrival is a modification of the primary wave, then

$$G_j(w)e^{-iw\lambda_j} = \left[A_j(w)e^{-iw\lambda_j}\right]\left[F_{out}(w)\right] \quad , \qquad (38)$$

where $A_j(w)e^{-iw\lambda_j}$ is the operator which when multiplied by the spectrum of the primary, yields the spectrum of the jth secondary arrival. Each operator has an amplitude and a phase distortion component as shown in equation (39).

$$A_j(w) = \left|A_j(w)\right| \; e^{i\alpha_j(w)} \quad , \qquad (39)$$

where: $\left|A_j(w)\right|$ = the amplitude distortion component of the operator for the jth secondary arrival ; and

$\alpha_j(w)$ = the phase distortion component of the operator for the jth secondary arrival.

If the calibration and unknown output signals observed at

a recording station are contaminated by N_c and N_u secondary arrivals, respectively, then the spectra of the observed (contaminated) output signals are related to the spectra of the uncontaminated output signals as shown in equations (40) and (41).

$$SC_{out}(w) = C_{out}(w)\left[1 + \sum_{j=1}^{N_c}\left|A_j(w)\right| e^{+i(\alpha_j(w) - w\lambda c_j)}\right] \quad (40)$$

$$SU_{out}(w) = U_{out}(w)\left[1 + \sum_{j=1}^{N_u}\left|B_j(w)\right| e^{+i(\beta_j(w) - w\lambda u_j)}\right], \quad (41)$$

where: $SC_{out}(w)$ = spectrum of the contaminated calibration output signal;

$C_{out}(w)$ = spectrum of the uncontaminated calibration output signal (primary wave);

$SU_{out}(w)$ = spectrum of the contaminated unknown output signal;

$U_{out}(w)$ = spectrum of the uncontaminated unknown output signal (primary wave);

N_c = number of secondary arrivals included in the calibration output signal;

$\left|A_j(w)\right|$ = amplitude distortion of the operator for the jth secondary arrival in the calibration output signal;

$\alpha_j(w)$ = phase distortion of the operator for the jth secondary arrival in the calibration output signal;

λc_j = delay time of the jth secondary arrival in the calibration output signal;

N_u = number of secondary arrivals included in the unknown output signal;

$|B_j(w)|$ = amplitude distortion of the operator for the jth secondary arrival in the unknown output signal;

$\beta_j(w)$ = phase distortion of the operator for the jth secondary arrival in the unknown output signal; and

λu_j = the delay time of the jth secondary arrival in the unknown output signal.

The input spectrum, $SU_{in}(w)$, that would be derived by the method of calibration using these contaminated output signals is related to the input spectrum that would be derived using only the pure primary waves, $U_{in}(w)$, as shown in equation (42).

$$SU_{in}(w) = U_{in}(w)\left[\frac{1 + \sum_{j=1}^{N_u} |B_j(w)| \; e^{i(\beta_j(w) - w\lambda u_j)}}{1 + \sum_{j=1}^{N_c} |A_j(w)| \; e^{i(\alpha_j(w) - w\lambda c_j)}}\right], \qquad (42)$$

where: $SU_{in}(w)$ = the unknown input spectrum that would be derived if secondary arrivals were included in the output signals;

$U_{in}(w) = \left[C_{in}(w) \frac{U_{out}(w)}{C_{out}(w)}\right]$ = the unknown input spectrum that would be derived if no secondary arrivals were included in the output signals; and

$C_{in}(w)$ = the spectrum of the calibration input signal.

When the spectra of the calibration and unknown output signals are modulated identically, then equation (42) reduces to equations (15) and (16) and the secondary arrivals would not affect the results of the method of calibration. However, it is clear, from equation (42), that differences in the amplitudes, waveforms, and/or delay times of secondary arrivals in the calibration and unknown output signals can affect the spectrum of the

input signal derived by the method of calibration. The amplitude and phase distortion components of the secondary arrival operators are, in general, unknown due to the complexity of the observed output signals. However, the possible effects of secondary arrivals on the applicability of the method of calibration can be illustrated by considering the reflections from the free surface at the sources.

Underground explosions are located in the proximity of a free surface, and it is possible that reflections from this free surface contaminate the primary waves. If the reflection coefficients at the free surface are independent of frequency, then for given angles of incidence, the amplitude distortion terms, $|A(w)|$ and $|B(w)|$, are constants R_c and R_u, respectively. The phase distortion terms, $\alpha(w)$ and $\beta(w)$, are equal to the constant π (radians), since for the angles of incidence considered in this research a signal reflected from the free surface is 180 degrees out-of-phase with the incident signal. The moduli of the surface reflection modulators (see equations 26, 40, and 41) are shown in Figure 20a (also see Figure 9a). The amplitude of the modulator increases as the reflection coefficient increases, while

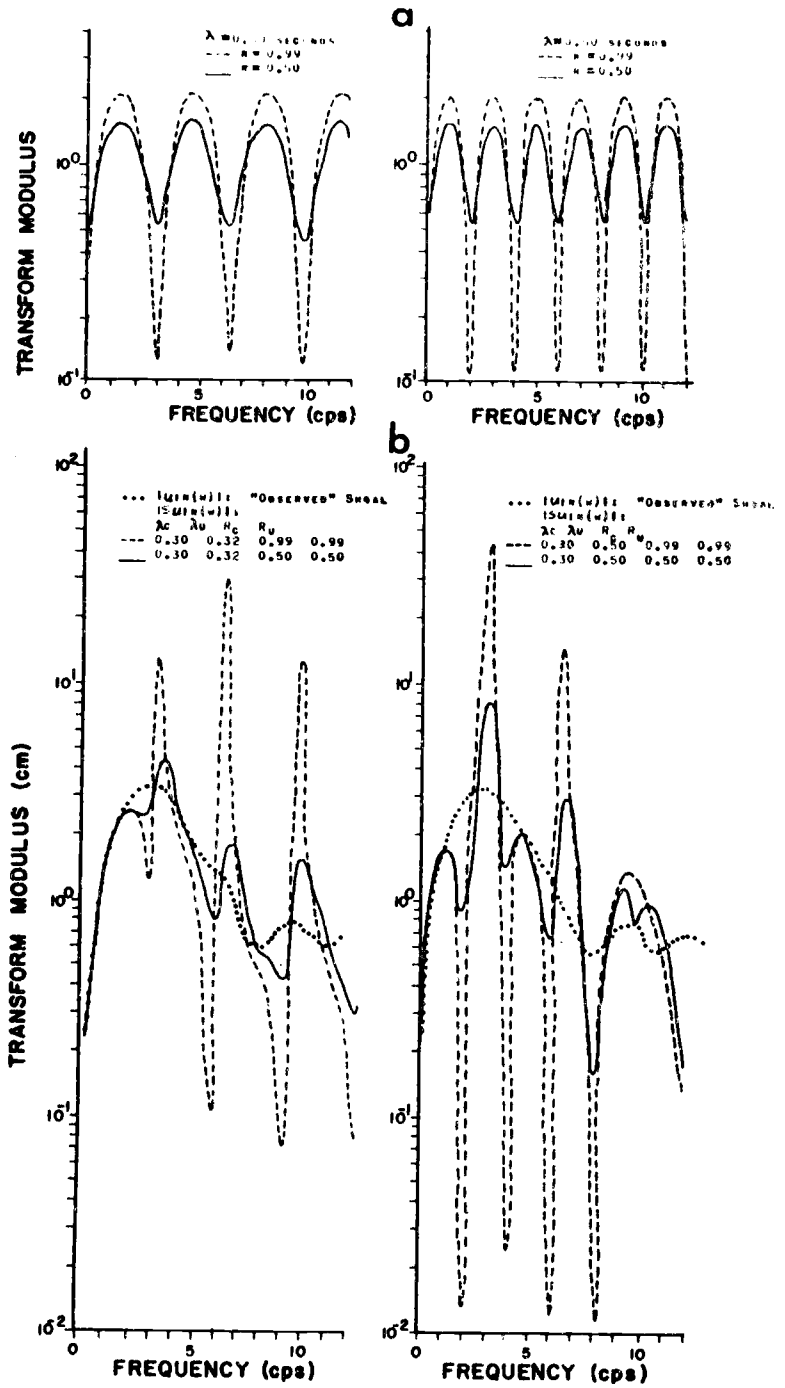

Figure 20. (a) Comparison of the moduli of the surface reflection modulators for delay times, λ = 0,30 and 0.50 seconds with reflection coefficients, |R| = 0.99 and 0.50. (b) Comparison of the spectral amplitudes of the observed source signal from the Shoal explosion to those that would be derived if surface reflections contaminate the output signals.

the repetition rate of the maxima and minima on the frequency axis decreases as the delay time decreases.

If no other secondary arrivals contaminate the output signals, then equation (42) reduces to:

$$SU_{in}(w) = U_{in}(w)\left[\frac{1 - R_u\, e^{-iw\lambda u}}{1 - R_c\, e^{-iw\lambda c}}\right]. \qquad (43)$$

The modulus of the input spectrum, $SU_{in}(w)$, that would be derived using the contaminated output signals is compared in Figure 20b to the modulus of the "observed" Shoal input spectrum, $U_{in}(w)$, for various values of the delay times (λc and λu) and reflection coefficients (R_c and R_u). It is clear that differences in the delay times of the reflections in the output signals can cause large variations in the amplitudes of the derived input spectrum. These variations increase as the reflection coefficients approach one (see Figure 20b). As the reflection coefficient, R_c, approaches one, the spectral amplitudes approach singularity (see equation 43) for the frequencies:

$$f = \frac{n}{\lambda c}\ , \text{ where: } \quad n = 0,1,2,\ldots\ldots\ldots, \qquad (44)$$

which is the reason that the reflection coefficients used in Figure 20b were less than one.

The energies and source functions obtained from the spectra in Figure 20b, using various frequency bandwidths, are shown in Figures 21 and 22. The source functions, $u_{in}(\tau)$ are the observed source signals for the Shoal explosion filtered with ideal low-pass filters for the indicated frequencies. The fundamental period used in the inverse transform was T = 5.0 seconds. The effect of the ideal low-pass filter, which is noncausal, is evident in the filtered observed signals. The source functions, $su_{in}(\tau)$, are the source signals that would be derived if surface reflections were included in the output signals with the indicated delay times and reflection coefficients.

The effect of the surface reflections on the derived source signals and source energy is pronounced when frequencies to 25 cps are used. The effect is most pronounced when the reflection coefficients are near one. However, in this research the high frequencies that could be utilized were limited by the attenuation of the earth. The broadest passband of frequencies that could be utilized was $0.2 \leqslant f \leqslant 4$ cps (near-regional station - MN-NV) and the narrowest passband was $0.2 \leqslant f \leqslant 2$ cps (teleseismic station - MBC). When the $su_{in}(\tau)$ are compared

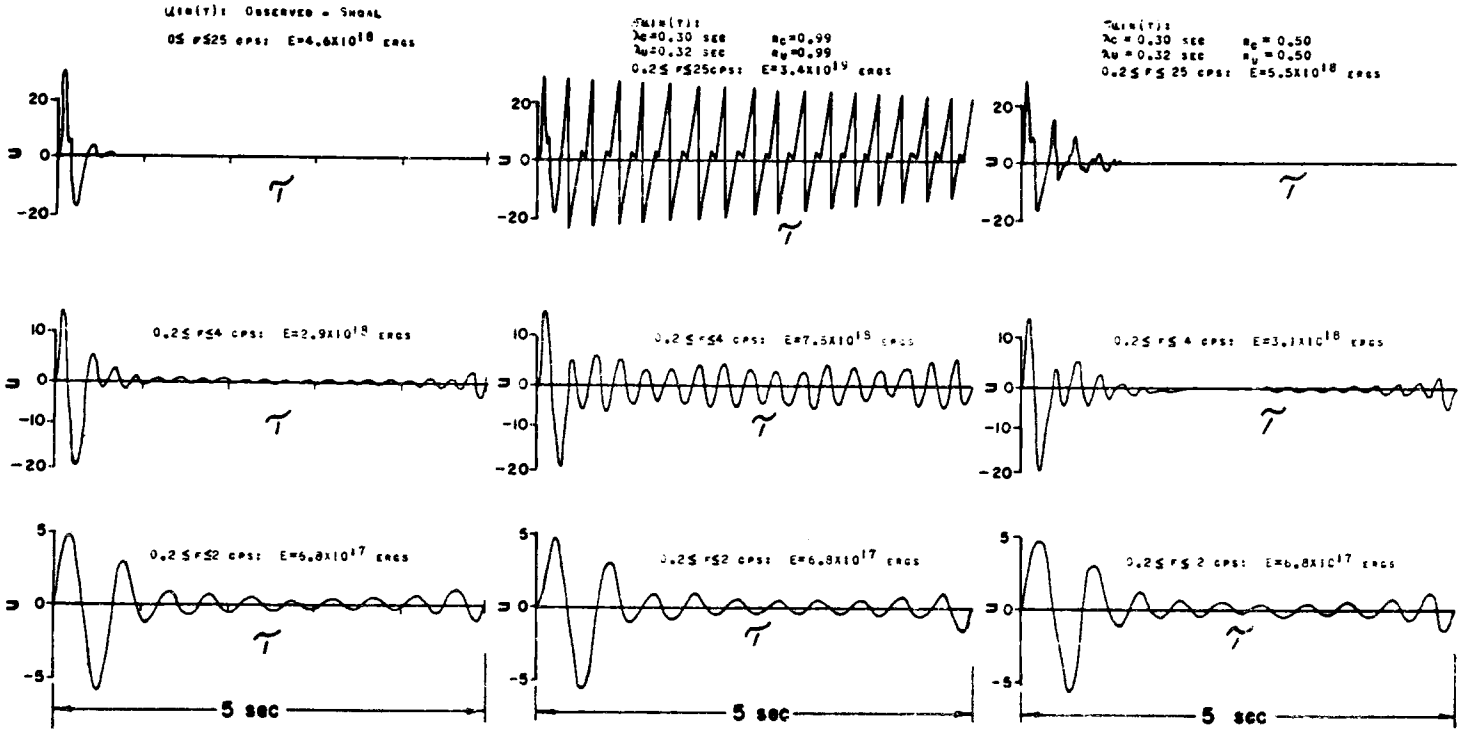

Figure 21. Comparison of the observed source signal (and energy) from the Shoal explosion to the source signal (and energy) that would be derived if surface reflections were included in the output signals (λ c = 0.30 seconds and λ u = 0.32 seconds).
u = particle velocity amplitude (cm/sec)
τ = reduced time in seconds.

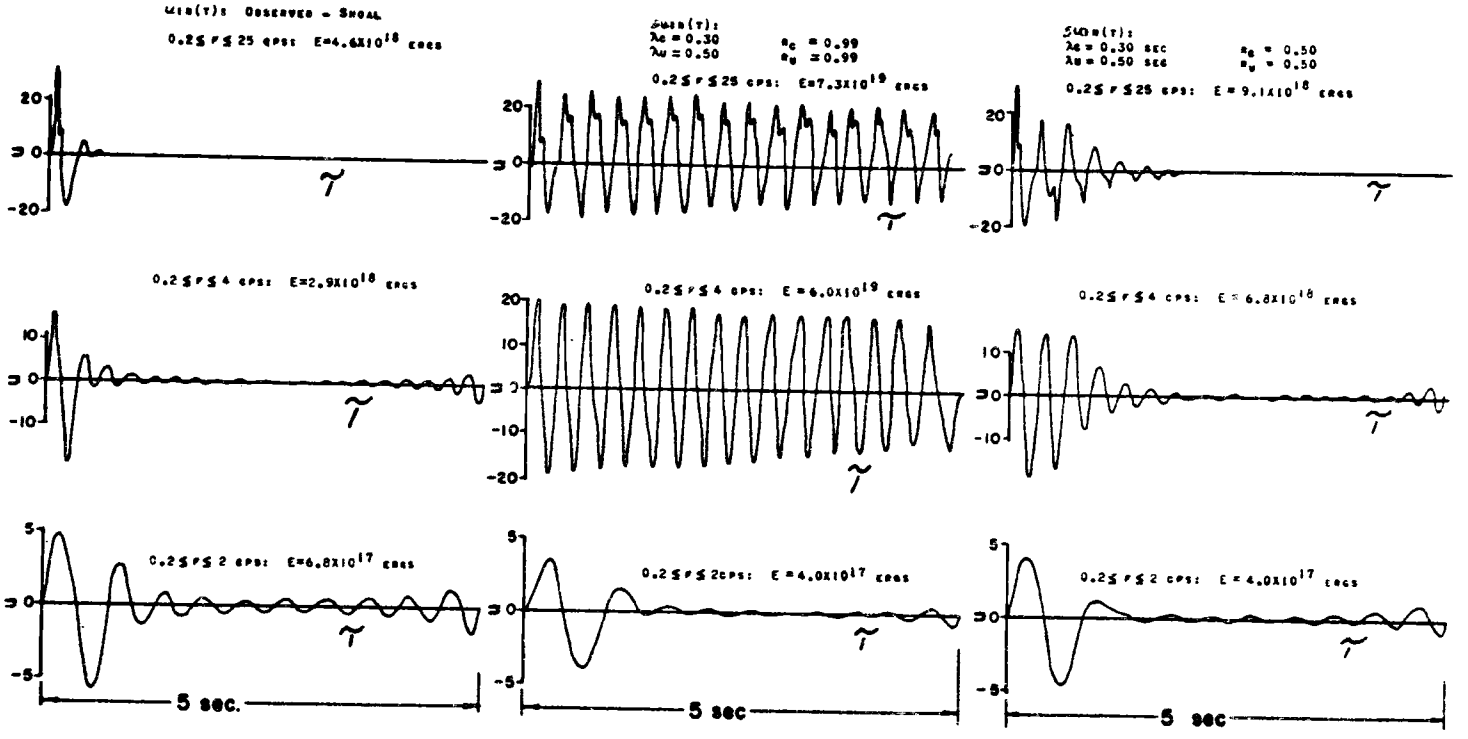

Figure 22. Comparison of the observed source signal (and energy) from the Shoal explosion to the source signal (and energy) that would be derived if surface reflections were included in the output signals ($\lambda c = 0.30$ seconds and $\lambda u = 0.50$ seconds).

u = particle velocity amplitude (cm/sec)

τ = reduced time in seconds.

to the $u_{in}(\tau)$ for these passbands, the effect of the differences in the surface reflections is not as pronounced (see Figures 21 and 22). However, it is clear that at near-regional stations, differences in the characteristics of surface reflections in the output signals can significantly affect the use of the method of calibration. Their effect is more pronounced as the reflection coefficients approach one. At teleseismic stations, the effects of the surface reflections do not greatly affect the use of the method of calibration, due to the narrow passband of frequencies contained in the output signals at that distance.

The effect of the surface reflections on the derived source functions can also be considered in the time domain. If the denominator in equation (43) is expanded in a complex binomial series, (for $|R|<1$), then

$$SU_{in}(w) = \left[U_{in}(w)\right]\left[1 - R_u e^{-iw\lambda u}\right]\left[\sum_{K=0}^{\infty} (R_c)^K e^{-iwK\lambda c}\right]. \quad (45)$$

The inverse transform of each of the quantities in brackets in equation (45) are shown in equations (46), (47), and (48).

$$T^{-1}\{U_{in}(w)\} = u_{in}(\tau), \tag{46}$$

$$T^{-1}\{1 - R_u e^{-iw\lambda u}\} = \delta(\tau) - R_u \delta(\tau - \lambda u), \tag{47}$$

$$T^{-1}\left\{\sum_{K=0}^{\infty} (R_c)^K e^{-iwK\lambda c}\right\} = \sum_{K=0}^{\infty} (R_c)^K \delta(\tau - K\lambda c), \tag{48}$$

where: $\delta(\tau)$ is the impulse function.

Since multiplication in the frequency domain implies convolution in the time domain, and since

$$A\delta(\tau - T_1) * B\delta(\tau - T_2) = A\,B\,\delta(\tau - T_1 - T_2),$$

(Papoulis, 1962), then

$$su_{in}(\tau) = \sum_{K=0}^{\infty} \left\{ \left[(R_c)^K u_{in}(\tau - K\lambda c) \right] - \left[R_u (R_c)^K u_{in}(\tau - \lambda u - K\lambda c) \right] \right\} . \tag{49}$$

Therefore, the source signal derived using output signals contaminated by surface reflections is an infinite series of positive and negative source signals. The delay times are dependent upon the delay times of the reflections in the output signals. The amplitudes of the source functions are dependent upon powers of the reflection coefficient of the surface reflection in the calibration

output signal. If this reflection coefficient is near one, tnen the amplitudes decrease slowly (i.e. the infinite series in equation 45 converges slowly). However, if the reflection coefficient is small, the amplitudes decrease rapidly (i.e. the infinite series in equation 45 converges rapidly). This effect is clearly evident in the source signals in Figures 21 and 22 for $0.2 \leqslant f \leqslant$ 25 cps. However, when the high frequencies of the source function $u_{in}(\mathcal{T})$ are removed, it is less impulsive and the positive and negative functions in equation (49) tend to cancel one another. The effect is, therefore, not pronounced when the high frequencies are not present in the source signals. This is also evident in Figures 21 and 22.